

DA-STC: Domain Adaptive Video Semantic Segmentation via Spatio-Temporal Consistency

Zhe Zhang¹, Gaochang Wu¹, Jing Zhang¹, Chunhua Shen², Dacheng Tao³, *Fellow, IEEE*,
Tianyou Chai¹, *Life Fellow, IEEE*

Abstract—Video semantic segmentation is a pivotal aspect of video representation learning. However, significant domain shifts present a challenge in effectively learning invariant spatio-temporal features across the labeled source domain and unlabeled target domain for video semantic segmentation. To solve the challenge, we propose a novel DA-STC method for domain adaptive video semantic segmentation, which incorporates a bidirectional multi-level spatio-temporal fusion module and a category-aware spatio-temporal feature alignment module to facilitate consistent learning for domain-invariant features. Firstly, we perform bidirectional spatio-temporal fusion at the image sequence level and shallow feature level, leading to the construction of two fused intermediate video domains. This prompts the video semantic segmentation model to consistently learn spatio-temporal features of shared patch sequences which are influenced by domain-specific contexts, thereby mitigating the feature gap between the source and target domain. Secondly, we propose a category-aware feature alignment module to promote the consistency of spatio-temporal features, facilitating adaptation to the target domain. Specifically, we adaptively aggregate the domain-specific deep features of each category along spatio-temporal dimensions, which are further constrained to achieve cross-domain intra-class feature alignment and inter-class feature separation. Extensive experiments demonstrate the effectiveness of our method, which achieves state-of-the-art mIOUs on multiple challenging benchmarks. Furthermore, we extend the proposed DA-STC to the image domain, where it also exhibits superior performance for domain adaptive semantic segmentation. The source code and models will be made available at <https://github.com/ZHE-SAPI/DA-STC>.

Index Terms—Domain adaptation, video semantic segmentation, feature alignment, spatio-temporal consistency.

I. INTRODUCTION

VIDEO semantic segmentation (VSS) aims at predicting pixel-level category for consecutive video frames, with significant applications in fields such as autonomous driving [1], [2], and industrial fault diagnosis [3], [4]. However, extensive manual annotation required for videos is laborious and time-consuming, which limits its practical applications. As a trade-off, training on label easily available synthetic videos rendered from computer engines is a promising manner.

Zhe Zhang, Gaochang Wu and Tianyou Chai are with the State Key Laboratory of Synthetical Automation for Process Industries, Northeastern University, Shenyang, China. Email: zhangzhe17@stumail.neu.edu.cn, wugc@mail.neu.edu.cn, tychai@mail.neu.edu.cn.

Chunhua Shen is with Zhejiang University, Hangzhou, China. E-mail: chhshen@gmail.com.

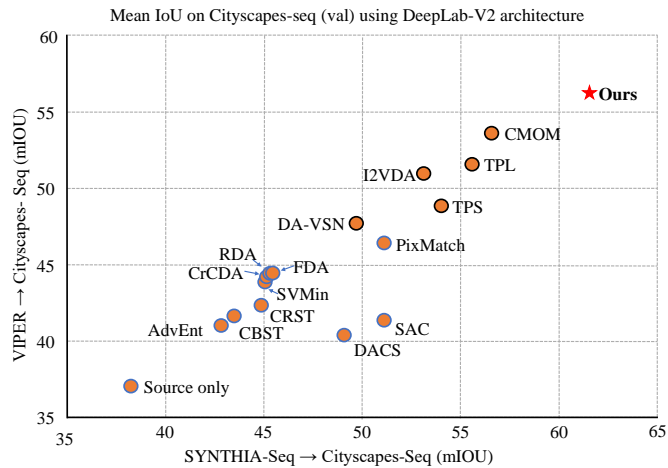
Jing Zhang and Dacheng Tao are with the School of Computer Science, in the Faculty of Engineering, at the University of Sydney, Sydney, Australia. E-mail: jing.zhang1@sydney.edu.au and dacheng.tao@sydney.edu.au.

Corresponding author: Tianyou Chai.

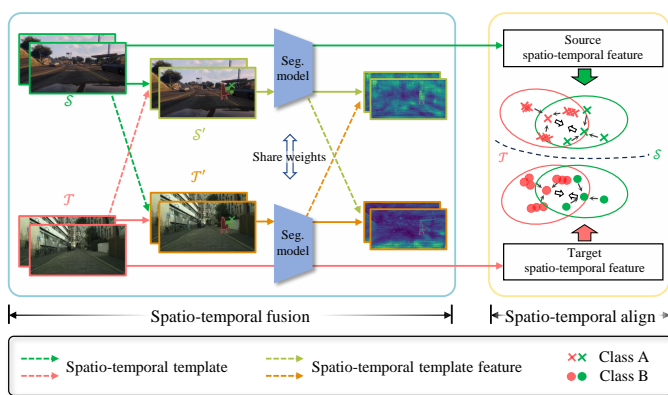
However, real-world objects always exhibit complex details in terms of color, style, texture, and even temporal characteristics, making it challenging for computers to simulate accurately. Directly applying such models to real unlabeled videos results in a notable performance drop due to large domain shift [5], [6].

In this work, we investigate Domain Adaptive Video Semantic Segmentation (DAVSS) to improve the model's transferability to the target video domain. Nevertheless, current research primarily focuses on images, which have limitations in robustly predicting coherent video semantics. Prior works [7], [8] aim to align cross-domain marginal distribution using adversarial methods. Long et al. [9] further incorporate multiple discriminators to align conditional probability distributions. Another line emphasizes self-supervised learning, which generates pseudo labels for the target domain through confidence estimation [10], consistency learning [11], or denoising [12]. Additionally, enhancing cross-domain feature alignment through addressing statistical distribution discrepancies along with the variants [5], [13], [14] have improved the adaptability of image semantic segmentation models. However, the straightforward division of videos into independent images often results in a performance drop [15], which can be attributed to the disregard for the inherent temporal attribute of video sequences. To capture inter-frame temporal dependencies, many innovative techniques have been explored in the VSS field, such as optical flow warping [16], inter-frame feature propagation [17], and attention mechanisms [18], which have achieved remarkable success. However, these approaches commonly rely on extra labels, especially for the key frames [19]. Moreover, VSS tailors for videos that share similar features, posing challenges in adapting to unlabeled target videos with large domain shifts. To facilitate knowledge transfer in videos, domain adaptive video action recognition [20], [21], [22] methods seek to learn constant temporal information from consecutive frames across the source domain and the target domain. While these studies demonstrate notable accuracy in sparse classification, yet encounter difficulties in fulfilling the demand for precise segmentation of pixel-level categories in video frames.

To fill this gap, domain adaptive video semantic segmentation has been explored in preliminary works. The key challenge is to learn domain-invariant spatio-temporal features across labeled source videos and unlabeled target videos to mitigate the domain gap. DA-VSN [15] first proposes temporal consistency regularization based on GAN, aiming to improve both the temporal consistency and prediction confidence of tar-



(a) Preview of the results on two challenging synthetic-to-real video semantic segmentation tasks.



(b) A brief illustration of DA-STC. We not only propose a multi-level spatio-temporal fusion module for consistent learning across domains, but also emphasize the class-aware aggregation and alignment of spatio-temporal features (illustrated with two categories).

Fig. 1. In (a), the points with blue edges represent image domain adaptation algorithms retrained with a video domain adapted segmentation network consistent with [15], [23], [24], and the points with black edges represent the recent DAVSS methods. Our method is shown with a red star. In (b), the colored dashed lines represent multi-level spatio-temporal templates transfer, and the constructed S' and T' exhibit a smaller domain gap compared to the original domains S and T . The self-supervised process with labels is omitted.

get frames. However, the training processes are characterized by instability due to synchronization of convergence problems. Subsequently, TPS [23] employs optical flow to warp prediction maps as pseudo labels for the subsequent target frames. Nevertheless, the learning of invariant cross-domain features is neglected. Furthermore, Cho et al. [24] introduce a stage-wise method for pseudo-label fine-tuning while incorporating spatial information from the source domain. In this process, the warm-up model in [15] is utilized to generate pseudo labels and initialize the model parameters. Recently, [25] suggests that cross-domain discrepancy in motion information is relatively minor compared with spatial features. Thus, robust optical flow could be utilized to enhance the reliability of pseudo labels. Moreover, Wu et al. [26] investigate the transfer of spatial knowledge from the image source domain to the video target domain, but overlook the valuable temporal features in source videos. Generally, existing methods can hardly solve the aforementioned key challenge. To overcome

the challenge, we emphasize the consistent learning of both spatial and temporal invariant features, leading to a substantial improvement in the target domain.

In this paper, we propose a novel Domain Adaptive Spatio-Temporal Consistency (DA-STC) method that incorporates bidirectional fusion at multiple levels and category-aware feature alignment to promote spatio-temporal consistency for domain adaptive video semantic segmentation, as illustrated in Fig. 1 (b). Firstly, we design a Bidirectional Spatio-Temporal Fusion (BSTF) module at the image sequence level, optical flow level and shallow feature level. Specifically, we carefully select variable category-specific spatio-temporal templates from source patches as well as target patches with high prediction confidence. The templates are then bidirectionally fused to source and target input sequences, along with shallow features and inter-frame optical flow fused in a similar way. This process establishes two fused intermediate domains, which share identical local semantics but exhibit distinct styles within respective contexts. By joint learning of the two intermediate domains supervised by corresponding fused labels, the proposed BSTF module effectively mitigates the cross-domain spatio-temporal feature discrepancy, thereby improving the generalization to the unlabeled target videos.

Secondly, we propose a category-aware spatio-temporal feature alignment module for the deep feature level to promote the consistency of the output feature space. Instead of implicitly focusing on the marginal distribution of the whole spatial feature [27], [28], we explicitly emphasize aligning conditional distribution of cross-domain spatio-temporal features on a per-category basis. To this end, we introduce a mapping operation to assign consecutive warped spatial features of previous time steps to various category-aware subdomains, which are then aggregated along the temporal dimension using entropy confidence weights. The category-aware aggregative spatio-temporal features of both domains are converted to the reproducing kernel Hilbert space, enabling the alignment of conditional probability distribution in the deep feature space between the source domain and the target domain.

The contributions of this paper can be summarized as follows:

- We propose a novel DAVSS method named DA-STC including a bidirectional spatio-temporal fusion module at the image sequence level, optical flow level, and shallow feature level, as well as a category-aware spatio-temporal feature alignment module at the deep feature level.
- The proposed BSTF module contributes to learning spatio-temporal consistency of the shared video semantics with domain-specific contexts. Moreover, the category-aware spatio-temporal feature alignment module enhances the cross-domain spatio-temporal consistency of conditional probability distributions, thus assisting in the adaptation to the target domain.
- Extensive experiments on challenging benchmarks demonstrate the superiority of our method. As shown in Fig. 1 (a), DA-STC obtains mIoUs of 61.5% and 56.2% on SYNTHIA-Seq [29] \rightarrow Cityscapes-Seq [30] and VIPER [31] \rightarrow Cityscapes-Seq, respectively. Ablation studies with detailed analysis verify the effectiveness

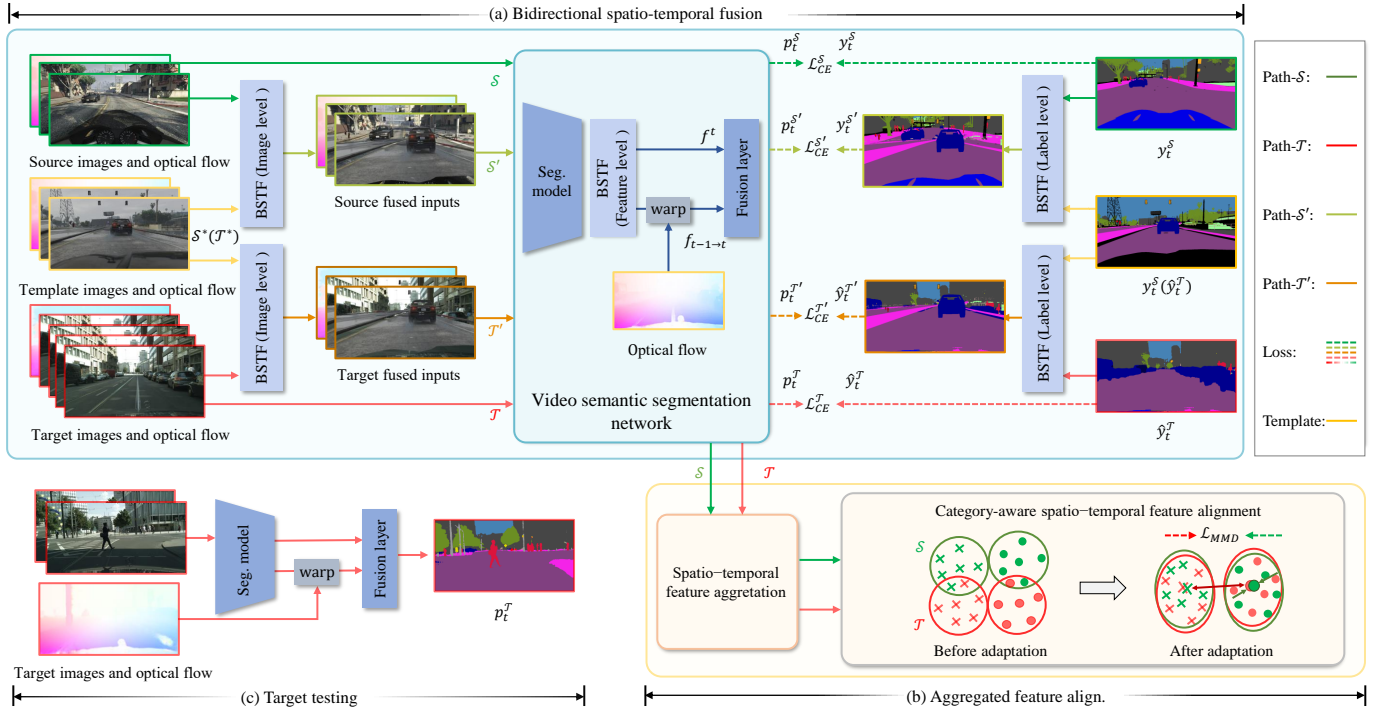


Fig. 2. An overview of our DA-STC method. We propose a novel DA-STC method involving a bidirectional spatio-temporal fusion (BSTF) module and a category-aware spatio-temporal feature alignment module. (i) As shown in part (a), we conduct bidirectional spatio-temporal fusion at the input sequence level and the optical flow level. We promote the consistent learning of two constructed intermediate domains that share identical local semantics but have distinct spatio-temporal contexts. (ii) In part (b), we assign consecutive optical warped spatial features to several category-aware subdomains, which are then aggregated along the temporal dimension, thereby facilitating subsequent alignment of the conditional probability distribution. Notably, pseudo-labels for frame t in the target domain are generated by warping the predicted map of frame $t - \tau$ using optical flow, ensuring the prediction consistency. (iii) Furthermore, during testing phase (c), it is only needed to input the image sequence and optical flow into the model to obtain the semantic segmentation result for frame t . Our method effectively promotes consistent learning of cross-domain invariant spatio-temporal features.

of each component.

- Furthermore, we extend our proposed DA-STC to image semantic segmentation, and the experiments demonstrate that it also exhibits superior performance for domain adaptive semantic segmentation.

II. RELATED WORK

A. Video Semantic Segmentation

VSS is a fundamental task that entails pixel-level classification for consecutive frames. With the development of deep convolutional neural networks and the availability of large-scale labeled data, VSS has gained widespread applicability [32], [33]. Mainstream works concentrate on leveraging temporal relationships among adjacent frames for accurate segmentation. For instance, the utilization of optical flow-guided feature warp [34] or prediction warp [35], along with temporal information propagation with recurrent network [36] or well-designed auxiliary network [37], have been developed. Additionally, Sun et al. [38] propose a coarse-to-fine method to capture both valuable static and dynamic contextual features. To improve inference efficiency, Hu et al. [39] suggest distributing several weight-sharing subnetworks across frames and reconstructing the extracted spatial features using attention mechanisms [40]. Recently, semi/weakly-supervised VSS have gained increasing attention. Lao et al. [41] propose a feature

enhancement network that models both short-term and long-term temporal dependencies. IFR [42] introduces novel feature reconstruction to mitigate inner-video overfitting, and leverages partial labels to supervise learning of unlabeled frames.

Notably, the manual annotation for real-world video segmentation is laborious and costly [43]. To reduce reliance on labels, we aim to transfer knowledge from the source model trained with label-rich synthetic videos to the label-scarce target videos in the real world. However, empirical studies [15], [23], [24], [25] have revealed that such models suffer considerable performance drop when directly applied to target videos due to large domain gap. To address this, we propose an effective domain-invariant spatio-temporal feature learning method that fosters accurate and robust semantic segmentation for target domain.

B. Domain Adaptive Image Semantic Segmentation

Domain adaptation for image semantic segmentation has received considerable attention in both theoretical and practical research. To improve the transferability to the target domain, many works concentrate on cross-domain invariant learning at image-level [44], [45], feature-level [46], [47], [48], and output-level [49], [50].

At the image sequence level, the key concept is to transfer the styles between two domains while preserving pixel-level semantics. Various approaches involving cycle translation [51], patch adversarial [52], domain invariant structure

extractor [53], and conditional GAN [54] have been proposed to facilitate cross-domain adaptive learning in terms of overall or local appearance styles. At the feature level, extensive research explores minimizing the distribution discrepancy between two domains. Influential metrics such as MMD [13], CORAL [14], and WD [55] have been utilized to reduce the distance of feature distribution across domains. Another recent development is the use of prototypes to represent feature centroids of different classes across domains, making significant contributions to methods such as pseudo label denoising [56], the design of feature divergence measurement [12], and cross-domain contrastive learning [48]. At the output level, adversarial adaptation on the low-dimensional prediction space using prediction maps has been proposed in [50]. To generate accurate target pseudo labels, some works propose progressive confidence [57] and curriculum learning [58], [59]. These approaches aim to provide the target domain with precise self-supervised information at the structured output space [60].

For DAVSS, considering consecutive frames as independent images is a natural idea, but it may overlook the utilization of temporal inherent information in videos. To effectively learn domain-invariant spatio-temporal features, we propose a BSTF module to perform cross-domain fusion at the input level, spatio-temporal feature level, and output level, as well as a category-aware spatio-temporal feature alignment module. This reduces the domain gap and enhances adaptation to the target video domain.

C. Domain Adaptive Video Semantic Segmentation

Research on video domain adaptation initially emerged from video action recognition [20], [21], [22], which involves sparse action classification for whole video clips. Recently, there has been a growing interest in domain adaptation for VSS. Guan et al. [15] firstly propose an adversarial learning method to effectively extract domain-specific temporal features that are difficult for discriminators to distinguish. This work also guides uncertain target predictions to have a similar tendency as confident adjacent predictions. It is noted that the asynchronous convergence of the generator and discriminator often leads to training instability. TPS [23] further introduces a self-supervised learning method that utilizes optical flow to warp prediction map from the previous frame as the current pseudo label. The model is trained alternately using source and target data without considering the interaction of two domains. Cho et al. [24] propose a staged pseudo label refinement method by generating initial pseudo labels and initializing model parameters based on a warm-up model provided in [15]. They also transfer source spatial information to the target domain. However, this work heavily relies on the well-trained initial model. Meanwhile, TPL [25] observes that optical flow, which captures video motion signals, exhibits smaller domain discrepancy compared to spatial features. Thus, they design pseudo labels based on robust optical flow for target domain self-supervision. By contrast, Wu et al. [26] argue that temporal information from the source domain is not necessary, and transferring only spatial information can also achieve effective generalization to the target videos.

In this paper, we highlight the significance of both spatial and temporal information for domain invariant learning. We present a novel end-to-end DA-STC method that integrates effective bidirectional spatio-temporal fusion and category-aware spatio-temporal feature alignment. Our method promotes the consistency of identical semantics across diverse spatio-temporal contexts and reduces the distribution discrepancy of cross-domain features, thereby achieving superior performance on the unlabeled target video domain.

III. METHOD

A. Method Overview

For DAVSS, we propose a method called DA-STC that emphasizes the importance of cross-domain spatio-temporal consistency learning. DA-STC consists of two key components: a bidirectional spatio-temporal fusion module and a category-aware spatio-temporal feature alignment module. Given a labeled source domain video V^S and an unlabeled target domain video V^T , our objective is to enhance the learning of domain-invariant spatio-temporal features, aiming to foster the model's adaptation to the target domain as well. As illustrated in Fig. 2, the model's input includes a frame pair along with the corresponding optical flows, denoted as $X_t^S = \{x_{t-1}^S, x_t^S\}$ and $o_{t-1 \rightarrow t}^S$ for the source domain and $X_{t-\tau}^T = \{x_{t-\tau-1}^T, x_{t-\tau}^T\}$ and $o_{t-\tau-1 \rightarrow t-\tau}^T$ for the target domain, as well as $X_t^T = \{x_{t-1}^T, x_t^T\}$ and $o_{t-1 \rightarrow t}^T$, where $\tau \geq 1$ corresponds to a frame interval generation for pseudo labels. Meanwhile, the model's output is the segmentation result of the latter frame t . In this paper, uppercase symbols denote sequences, whereas lowercase symbols signify an individual frame.

Firstly, in part (a), we perform bidirectional fusion at multiple levels, including the image sequence, inter-frame optical flow, shallow feature, and label levels. The proposed fusion module establishes two intermediate video domains, $V^{S'}$ and $V^{T'}$, with relatively smaller domain gaps compared with the original ones. At the image sequence level, as depicted on the left side of part (a), we adaptively generate sequence templates Z_t that incorporate category-aware patch sequences from both source and target with high-confidence predictions. Subsequently, Z_t is bidirectionally fused into X_t^S and X_t^T to generate two fused intermediate sequences $X_t^{S'}$ and $X_t^{T'}$. The fused image sequences and corresponding fused optical flows are fed into the video semantic segmentation network, yielding the semantic segmentation map p_t' for frame t . The BSTF module at the feature-level is also performed as depicted in the middle of part (a). The training loss is then calculated based on the predicted $p_t^{S'}$, $p_t^{T'}$, and the corresponding fused label $y_t^{S'}$, $\hat{y}_t^{T'}$, respectively.

Secondly, we propose a category-aware spatio-temporal feature alignment module, as illustrated in part (b) of Fig. 2. To effectively exploit the continuity of spatio-temporal context, with the assistance of optical flow, we use optical flow to warp the source per-frame spatial features f_{t-1}^S to the current time t , yielding $f_{t-1 \rightarrow t}^S$. Similarly, we acquire $f_{t-\tau-1 \rightarrow t}^T$, $f_{t-\tau \rightarrow t}^T$, and $f_{t-1 \rightarrow t}^T$ from the target domain. The cross-frame warped spatial features are input into the category-aware video feature

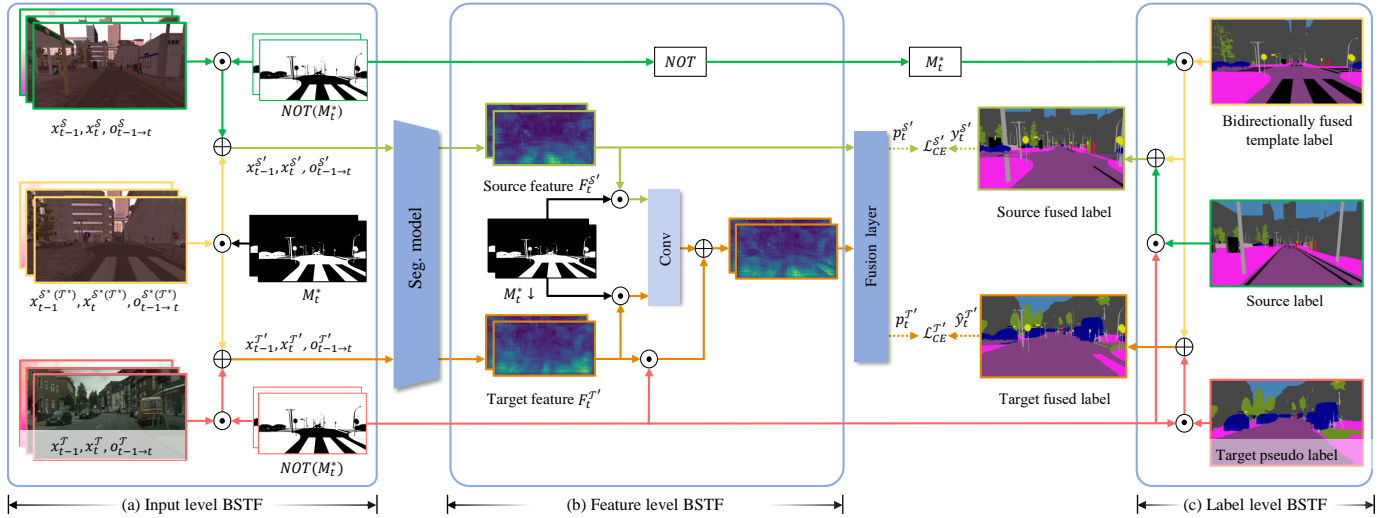


Fig. 3. Illustration of the BSTF module. The fusion process is conducted at multiple levels including input image sequences, inter-frame optical flow, shallow features, and label sequences, constructing two closer intermediate domains. Our goal is to learn invariant spatio-temporal features that are not influenced by domain-specific contexts. The mask M_t^{S*} may denote the source mask M_t^{S*} or target mask M_t^{T*} .

aggregation module. In this module, fused spatio-temporal features are initially mapped into multiple category subdomains and then aggregated along the temporal dimension. Subsequently, we project the final aggregated features into the reproducing Hilbert space to minimize the maximum mean difference across domains.

B. Basic Bidirectional Spatio-Temporal Fusion

Despite the similarities in semantic labels between the source and target domain videos, a significant domain gap often exists in style, content, and even semantic coherence, which can result in poor generalization on unseen target domains. Instead of simply alternating the training between the two domains [23], we propose a cross-domain bidirectional spatio-temporal feature fusion module at the image sequence level, optical flow level, and feature level. Fig. 3 presents a comprehensive depiction of the BSTF module. The constructed intermediate video domains simultaneously incorporate bidirectional spatio-temporal contextual information from both synthetic and real domains, which contributes to cross-domain consistency learning. In this section, we present the proposed basic BSTF.

1) Bidirectional Input Level Fusion with Source Template:

At the input level, the term *bidirectional* means the dynamic sequence templates Z are bidirectionally fused with the image sequences X^S and X^T within each training step to construct two intermediate sequences. The optical flows can be bidirectionally obtained in a similar way. In this section, we propose the basic scenario where templates are from the source domain, as shown in Fig. 1 (b) but excluding the information transmission represented by the red dashed line.

Source-to-target fusion. At the image sequence level, we initiate the process by extracting the category-aware patch sequence from video sequence $Z_t^{S*} = \{x_{t-1}^{S*}, x_t^{S*}\}$ in the last training step using label priors, where S^* refers to the source data in the last training step. Specifically, we randomly select a

subset of categories from the whole source category space K^S of the current training batch and utilize a binarization operation to generate corresponding category masks M_t^{S*} . This process can be formalized as:

$$M_t^{S*} = \mathbb{1}(Y_t^{S*} == k), k \in K^S, \quad (1)$$

where $\mathbb{1}(\cdot)$ is the indicator function. Note that $M_t^{S*} = \{m_{t-1}^{S*}, m_t^{S*}\}$ since our fusion strategy is operated on consecutive frames, each spatial mask m has a size of $B \times H \times W$ and comprises binary value, where B means the batch size.

We dynamically map the source template sequence Z_t^{S*} using M_t^{S*} , and simultaneously map the target domain sequence X_t^T in the current training step using the complementary part. The results of both mappings are then combined to form the fused target domain initially. The fusion process is illustrated as follows:

$$X_t^{T'} = Z_t^{S*} \odot M_t^{S*} + X_t^T \odot (1 - M_t^{S*}), \quad (2)$$

where \odot refers to a position-wise multiplication operation.

Apart from image sequences, the consideration of optical flow, which reflects the motion relationship within frames, is essential for the bidirectional fusion. Following the mechanism similar to Eq. (1) and (2), we integrate optical flow from the source domain to generate fused optical flow $o_{t-1 \rightarrow t}^{T'}$ of intermediate target domain. Specifically, we replace the image sequences X_t and Z_t with the inter-frame optical flow $o_{t-1 \rightarrow t}$, and substitute the mask sequence M with the spatial mask m_{t-1} , as the optical flow is propagated from frame $t-1$ to frame t .

Source-to-source fusion. In a similar manner, the fused image sequence $X_t^{S'}$ of the intermediate source domain can be generated by substituting X_t^S for X_t^T and $X_t^{S'}$ for $X_t^{T'}$ in Eq. (2). Additionally, the fused optical flow $o_{t-1 \rightarrow t}^{S'}$ could also be adaptively generated. Through input level fusion, the two constructed sequences $X_t^{S'}$ and $X_t^{T'}$ comprise identical patch sequences, yet the shared semantics possess distinct spatio-temporal contextual environments exclusive to the source and

target domains. The joint learning of spatio-temporal features in two fused intermediate video domains contributes to reducing the domain gap between the original source domain S and the target domain T , thereby enhancing the transferability to the latter.

2) *Bidirectional Feature Level Fusion*: Considering the design that fused intermediate domains encompass shared patch templates from both source and target domains, we encourage the video semantic segmentation model to ignore the domain-specific style in spatio-temporal contexts and prioritize acquiring robust semantic information in the feature space. As depicted in Fig. 3 (b), We adaptively perform feature fusion at a relatively shallow level of two fused domains to enhance the model’s learning capability for diverse spatio-temporal features. Firstly, the feature mask $M_t^* \downarrow$ is utilized to map shallow features $F_t^{S'}$ from the intermediate source domain, and then the mapping results are integrated with target feature $F_t^{T'}$. The process is formulated as:

$$F_t^{T'} \leftarrow \text{conv}(F_t^{S'} \odot M_t^* \downarrow, F_t^{T'} \odot M_t^* \downarrow) + F_t^{T'} \odot (1 - M_t^* \downarrow), \quad (3)$$

where the binary patch feature mask $M_t^* \downarrow$ is downsampled from the integrated M_t by linear interpolation due to memory constraints. In this section, M_t is equal to the source mask $M_t^{S^*}$. Consequently, the fused target features $F_t^{T'}$ are then input into the Atrous Spatial Pyramid Pooling (ASPP) [61] module.

In this way, we attempt to prompt the model to learn the consistent feature of the shared semantics across two fused intermediate domains despite their distinct spatio-temporal contexts. Notably, partially supervised information of source patch sequence in the fused target domain promotes learning robust spatio-temporal features.

C. Generalized Bidirectional Spatio-Temporal Fusion

1) *Scaling BSTF Paradigms with Target Template*: Apart from the one in Section III-B1, the term *bidirectional* has another aspect: the generation of the template sequences Z involves the fusion of category-aware patch sequences which are bidirectional from the source and target domains. To further mitigate the domain gap, in this section, we propose more generalized BSTF paradigms corresponding to Fig. 1 (b), with specific details shown in Fig. 3.

Target-to-source fusion. Naturally, we associate that the evolving pseudo masks could also offer essential information for the model [62]. Therefore, it would be beneficial if two intermediate domains also incorporate information from the target domain. Considering the low target accuracy of the model in initial training steps, we introduce a filtering mechanism using threshold γ compared with predicted logits to obtain the confident category-aware target pseudo masks, which yields $\hat{M}_t^{T^*}$ corresponding to $Z_t^{T^*}$ from the last training step iteratively in a manner similar to Eq. (1). To alleviate pixel overlap in multiple template sequences as much as possible, we ensure that the source category space K^S and the target category space K^T are mutually exclusive. The updated fused source domain sequence is as follows:

$$X_t^{S'} \leftarrow Z_t^{T^*} \odot \hat{M}_t^{T^*} + X_t^{S'} \odot (1 - \hat{M}_t^{T^*}) \quad (4)$$

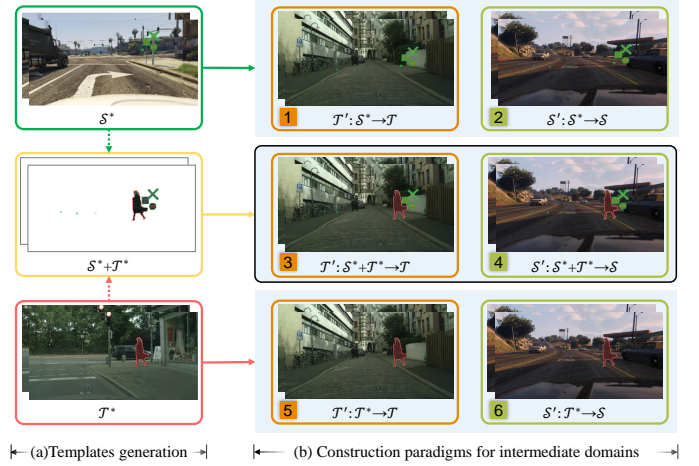


Fig. 4. Illustration of the generation for templates and construction paradigms for intermediate domains. For simplicity, we choose the categories *person* and *sign* as examples. In part (a), S^* and T^* represent the source templates and target templates, respectively, highlighted with colored masks. Part (b) displays the nine construction paradigms for fused intermediate domains, including the construction of single fused source domain S' with orange boxes (2, 4, 6), or T' with green boxes (1, 3, 5), and the combination of two fused domains marked with blue backgrounds ((1,2), (3, 4), (5, 6)). Each of these nine paradigms effectively reduces the domain gap, and the combination of two fused domains tends to yield better results. Notably, paradigm (3, 4) achieves the best performance. Best viewed in color.

where $M_t^{T^*}$ is derived based on continually evolving pseudo labels $Y_t^{S^*}$, following a mode akin to Eq. (1).

Target-to-target fusion. Furthermore, we perform the fusion of target templates in the last training step with the target image sequence in the current step. The updated intermediate target sequence $X_t^{T'}$ is generated analogous to Eq. (4) by replacing $X_t^{S'}$ with $X_t^{T'}$. An intriguing observation is that the confidence-based filtering mechanism efficiently identifies more reliable target templates. Consequently, the enhanced accuracy of target templates fused to two domains effectively reduces the gap between the intermediate source and target domains.

Consistent with Section III-B, the optical flows corresponding to the templates from target domain are further bidirectionally fused into two intermediate domains. During the feature fusion process, the integrated mask M_t in Eq. (3) is updated to the intersection of $M_t^{S^*}$, $M_t^{T^*}$, and M_t^S . In terms of label-level fusion, we merge the source labels y_t^S and the target pseudo labels \hat{y}_t^T using a similar approach as in Eq. (1) and Eq. (4), in which X and Z just be replaced by y , and the mask sequence M is replaced with the mask m_t for the latter frame. Notably, we employ optical flow to generate cross-frame consistent pseudo label for target self-supervised learning.

Comprehensively, the template Z in Eq. (2) and Eq. (4) can be a spatio-temporal template from either the source or target domain, or it can be optical flow or semantic segmentation label. The flexibility inspires us to propose various scalable paradigms for BSTF. As depicted in Fig. 4, taking image sequences as an example, we create three kinds of temporal patch templates: source templates, target templates, and templates from both domains simultaneously. Based on these templates,

we propose nine construction paradigms for intermediate domains, involving the construction of a single fused target domain, a single fused source domain, and the combination of two fused intermediate domains simultaneously. Remarkably, in the case of SYNTHIA-Seq \rightarrow Cityscapes-Seq, the performance of all nine paradigms surpasses the state-of-the-art CMOM [24] with an mIOU of 56.3%, as verified by extensive ablation studies in Table VI. Moreover, the paradigm with the combination of bidirectional templates and bidirectional fused intermediate domains achieves the best mIOU of 61.5%, highlighted with a black box in Fig. 4. Further comparison and analysis of the aforementioned paradigms will be detailed in ablation studies. In conclusion, exploiting the consistency of the spatio-temporal features in these fused domains effectively reduces the feature discrepancy between the source and target domains.

2) *Discussion*: Our bidirectional spatio-temporal fusion module is comprehensive yet effective. In contrast to the recently proposed DACS [45], our method not only constructs a mixed target domain but also establishes a fused source domain, wherein the spatio-temporal features of shared semantics are adaptively fused. A distinguishing feature of our method compared to the most recent CMOM [24] and DSP [27] approaches is the incorporation of both source domain sequence templates and high-confidence target domain sequence templates. Furthermore, we carry out cross-domain feature fusion across fused intermediate domains. In addition, we further leverage the video’s temporal information to adaptively generate fused optical flows for two intermediate domains.

In addition, Cheng et al. [51] recently introduced a CycleGAN translation [63] based classmix method for image domain adaptive semantic segmentation. However, this work addresses category-level weighted samples for hard learning categories in the target domain, which may learn noisy spatial information during the early training stages. In contrast, our BSTF module targets pixel-level fusion with high confidence, along with relevant motion information, which aids the model in learning robust spatio-temporal features. Furthermore, [51] primarily emphasizes spatial-level mixing for images and employs a multi-stage training approach with two warm-up models for the source and target domains separately. In contrast, we perform bidirectional spatio-temporal fusion at multiple levels for video domain adaptation with a unified model. Additionally, our model could be trained without relying on warm-up models, resulting in fewer loss terms and more straightforward convergence.

Experimental results demonstrate that our BSTF module achieves relatively low computational cost while significantly enhancing transferability to target domain videos, with notable improvements across various categories, particularly in hard-to-transfer items.

D. Category-Aware Spatio-Temporal Feature Alignment

In this section, our goal is to mitigate cross-domain distribution discrepancy of spatio-temporal features at the deep feature level, thereby enhancing the consistency of the output feature space in both domains. Firstly, for self-supervised

learning of target videos, we employ optical flow to propagate information from previous frames to the current frame t as pseudo labels (see Section III-D1). Subsequently, based on the source label prior and target domain pseudo label, the spatio-temporal features across two domains are aggregated to category-aware subdomains separately, enabling the alignment of cross-domain subdomain features using maximum mean discrepancy (see Section III-D2).

1) *Spatio-Temporal Feature Extraction*: Similar to [15]-[25], we firstly adopt the ACCEL [34] as the architecture of the video segmentation network. The network structure \mathcal{G} involves two semantic segmentation branches and one optical flow branch. These shared-weight segmentation branches are used to capture deep spatial features from both domains. In this work, during the training forward of the fused intermediate inputs, we employ the BSTF at the feature level before the ASPP module. Additionally, the optical flows are computed offline using FlowNet [64] in line with [15] - [24]. The feature f_t and optical-warped feature $f_{t-1 \rightarrow t}$ are fed into a fusion layer ϕ_f to output the prediction map p_t . The process is described as follows:

$$p_t = \phi_f(f_{t-1 \rightarrow t}, f_t). \quad (5)$$

The warped feature from frame $t - 1$ to t is obtained by:

$$f_{t-1 \rightarrow t} = \mathcal{W}(f_{t-1}, o_{t-1 \rightarrow t}), \quad (6)$$

where \mathcal{W} is a warp operation using bilinear interpolation.

For unlabeled target videos training, given the inherent semantic continuity across video frames, we introduce an intra-domain cross-frame consistency learning method to generate pseudo labels. Consecutive frames $\{x_{t-\tau-1}^T, x_{t-\tau}^T\}$ from the target domain are fed into the segmentation network to output the prediction map $p_{t-\tau}^T$. Then, we generate pseudo labels \hat{y}_t^T by warping $p_{t-\tau}^T$ using optical flow $o_{t-1 \rightarrow t}^T$, as described as:

$$\hat{y}_t^T = \arg \max_k (\mathcal{W}(p_{t-\tau}^{T,(k)}, o_{t-1 \rightarrow t}^T)), \quad (7)$$

where k denotes the category index, and τ represents the frame interval generation for pseudo labels. The progressively refined pseudo labels will provide self-supervised information for augmented X_t^T and category-aware information.

For source domain training or target domain testing, as depicted in Fig. 2 (c), it is only needed to input the frame sequence $\{x_{t-1}, x_t\}$ and optical flow $o_{t-1 \rightarrow t}$ into network \mathcal{G} to obtain semantic segmentation results.

2) *Distribution Alignment of Category-Aware Features*: To enhance the alignment of cross-domain spatio-temporal conditional probability distributions, we propose a cross-domain temporal feature aggregative alignment method. Instead of implicitly treating cross-domain spatial features as a whole [27], we focus on the alignment of deep spatio-temporal features on a category bias, as shown in Fig. 5.

We firstly employ optical flows to warp the consecutive spatial features of both the source and target domains to the timestamp t , following Eq. (5) and Eq. (6). Then, taking the target domain as an example, upon merging the warped feature $f_{t' \rightarrow t}^T$ with the feature f_t^T through the fusion layer, we obtain the current frame deep feature $p_{t' \rightarrow t}^T$ containing

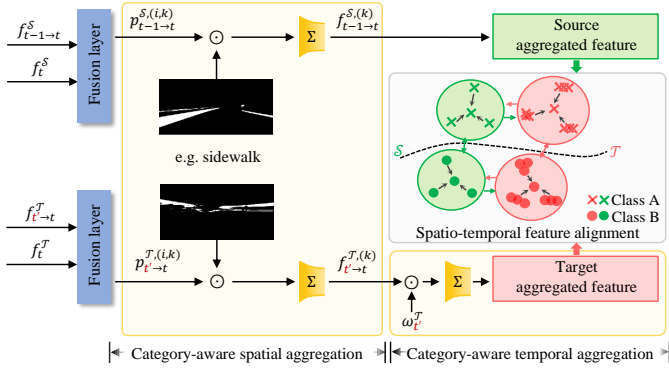


Fig. 5. The illustration of our category-aware spatio-temporal feature alignment module, where t' signifies previous time steps, and $\omega_{t'}^T$ denotes temporal aggregation weights of target frames. We denote p_t as $p_{t' \rightarrow t}$ to distinguish the features from previous time steps. The arrows represent the mean aggregation of category-aware features in the local training batch.

inner-frame information, with the past frame timestamp $t' \in \{t-1, t-\tau, t-\tau-1\}$. Subsequently, we adaptively generate category-aware masks for each category following a similar approach as in Eq. (1). Building upon this, we distribute the deep features to the category-wise subspaces, obtaining the source spatial feature $f_{t-1 \rightarrow t}^{S,(k)}$ and the target spatial features $f_{t' \rightarrow t}^{T,(k)}$, respectively, as described in Eq. (8) and Eq. (9):

$$f_{t-1 \rightarrow t}^{S,(k)} = \frac{\sum_{i=1}^{H \times W} (p_{t-1 \rightarrow t}^{S,(i,k)} \odot \mathbb{1}(y_t^{S,(i,k)} == k))}{\sum_{i=1}^{H \times W} \mathbb{1}(y_t^{S,(i,k)} == k)}, \quad (8)$$

$$f_{t' \rightarrow t}^{T,(k)} = \frac{\sum_{i=1}^{H \times W} (p_{t' \rightarrow t}^{T,(i,k)} \odot \mathbb{1}(\hat{y}_{t' \rightarrow t}^{T,(i,k)} == k))}{\sum_{i=1}^{H \times W} \mathbb{1}(\hat{y}_{t' \rightarrow t}^{T,(i,k)} == k)}, \quad (9)$$

where category k belongs to the whole category space K . In this way, the average aggregation of spatial features with non-zero objects corresponding to specific category k is obtained.

For target domain sequences, we compute the aggregated deep feature by assembling consecutive category-aware features along the timeline using the entropy confidence $\omega_{t'}^T$:

$$f_{t'}^{T,(k)} = \sum_{t'} f_{t' \rightarrow t}^{T,(k)} \cdot \omega_{t'}^T, \quad (10)$$

where $\omega_{t'}^T$ is obtained by softmax normalization among the confidence of adjacent frames, which is formulated as:

$$\omega_{t'}^T = \text{softmax}_{t'} \left(-\frac{1}{H \times W} \sum_i (-p_{t'}^{T,(i)} \cdot \log(p_{t'}^{T,(i)})) \right), \quad (11)$$

where the predicted confidence and the temporal weight $\omega_{t'}^T$ are positively correlated. In this work, we regard $f_{t-1 \rightarrow t}^{S,(k)}$ as the aggregated deep feature $f^{S,(k)}$ for source domain due to the accurate labels for supervision.

Subsequently, we concatenate the subdomain features of the two domains along the category dimension to obtain f^T and f^S , which are then converted to the reproducing Hilbert space

Algorithm 1 Domain Adaptive Video Semantic Segmentation via Spatio-temporal Consistency.

- 1: **Input:** Input data $X_t^S, X_t^T, X_{t-\tau}^T, o_{t-1 \rightarrow t}^S, o_{t-\tau-1 \rightarrow t-\tau}^T, o_{t' \rightarrow t}^T$, batch size B , parameters $\lambda_{\mathcal{T}}$ and λ_f and maximum iteration N .
- 2: Initialize the DA-STC model \mathcal{G} with ImageNet pre-trained parameters.
- 3: **for** $iter \leftarrow 0$ to N **do**
- 4: **if** $i == 0$ **then**
- 5: Generate the initial target pseudo $\hat{Y}_t^{T'}$ for the calculation of $\hat{M}_t^{T'}$ in the following iters.
- 6: **else**
- 7: Generate fused image sequences $X_t^{S'}$ for the intermediate source domain and $X_t^{T'}$ for the intermediate target domain via Eq. (1) - (4).
- 8: Generate fused optical flows $o_{t-1 \rightarrow t}^{S'}$ and $o_{t-1 \rightarrow t}^{T'}$.
- 9: Generate fused label sequences $y_t^{S'}$ and $\hat{y}_t^{T'}$.
- 10: Input $X_t^{S'}$ and $X_t^{T'}$ to model \mathcal{G} , perform shallow spatio-temporal feature fusion for two fused domains and obtain cross intermediate domain loss L_{BSTF} with $y_t^{S'}$ and $\hat{y}_t^{T'}$ via Eq. (13).
- 11: Perform category-aware spatio-temporal feature alignment and then compute the feature discrepancy of deep spatio-temporal features via Eq. (14).
- 12: Given X_t^S, X_t^T along with optical flows as input of model \mathcal{G} , calculate the cross-domain loss L_{ssl} with y_t^S and \hat{y}_t^T via Eq. (15).
- 13: Update parameters of \mathcal{G} using the overall loss L_{all} in Eq. (12).
- 14: **end if**
- 15: **end for**
- 16: **Output:** Final weights of the DA-STC model.

as shown in Fig. 5. By minimizing the MMD (maximum mean difference) loss $\|\mu^S - \mu^T\|_{\mathcal{H}}^2$ [13], we aim to reduce intra-category feature discrepancy while increasing inter-category feature differences. Extensive experiments have demonstrated the effectiveness of our approach in improving the transferability to the target videos.

E. Training Procedure and Objective Optimization

Our method follows a self-supervised learning paradigm, and the overall training procedure is summarized in Algorithm 1. The overall loss function is defined as follows:

$$\mathcal{L}_{all} = \mathcal{L}_{BSTF} + \mathcal{L}_{align} + \mathcal{L}_{SSL}, \quad (12)$$

which includes \mathcal{L}_{ssl} for cross-domain self-supervised learning, \mathcal{L}_{BSTF} for cross-domain consistency learning, and \mathcal{L}_{feat} for deep spatio-temporal feature alignment.

BSTF loss. As shown in Fig. 3, we present the BSTF module for constructing two fused intermediate video domains. To exploit the consistent learning of the shared category-specific template sequences with domain-specific spatio-temporal contexts, we propose a loss as follows:

$$\mathcal{L}_{BSTF} = \mathcal{L}_{CE}^S(\mathcal{G}(X_t^{S'}, o_{t-1 \rightarrow t}^{S'}, y_t^{S'})) + \lambda_{\mathcal{T}} \mathcal{L}_{CE}^T(\mathcal{G}(X_t^{T'}, o_{t-1 \rightarrow t}^{T'}, \hat{y}_t^{T'})), \quad (13)$$

TABLE I

QUANTITATIVE RESULTS IN TERMS OF PER-CATEGORY IOU AND MIOU ON SYNTHIA-SEQ \rightarrow CITYSCAPES-SEQ. THE BEST RESULT IS HIGHLIGHTED IN BOLD WHILE THE BEST RESULT WITHOUT USING A WARM-UP MODEL IS UNDERLINED. ‘‘ADV.’’: ADVERSARIAL LEARNING, ‘‘SSL’’: SELF-SUPERVISED LEARNING, ‘‘WARM’’: USING A WARM-UP MODEL.

Methods	SYNTHIA-Seq \rightarrow Cityscapes-Seq			road	side.	buil.	pole	light	sign	vege.	sky	pers.	rider	car	mIOU
	Adv.	SSL	Warm												
Source only				56.3	26.6	75.6	25.5	5.7	15.6	71.0	58.5	41.7	17.1	27.9	38.3
AdvEnt [65]	✓			85.7	21.3	70.9	21.8	4.8	15.3	59.5	62.4	46.8	16.3	64.6	42.7
CBST [66]		✓		64.1	30.5	78.2	28.9	14.3	21.3	75.8	62.6	46.9	20.2	33.9	43.3
IDA [67]	✓			87.0	23.2	71.3	22.1	4.1	14.9	58.8	67.5	45.2	17.0	73.4	44.0
CRST [68]		✓		70.4	31.4	79.1	27.6	11.5	20.7	78.0	67.2	49.5	17.1	39.6	44.7
SVMin [69]				84.9	0.5	77.9	29.6	7.4	15.0	78.6	73.2	46.9	6.2	73.8	44.9
CrCDA [70]	✓			86.5	26.3	74.8	24.5	5.0	15.5	63.5	64.4	46.0	15.8	72.8	45.0
RDA [71]		✓		84.7	26.4	73.9	23.8	7.1	18.6	66.7	68.0	48.6	9.3	68.8	45.1
FDA [72]		✓		84.1	32.8	67.6	28.1	5.5	20.3	61.1	64.8	43.1	19.0	70.6	45.2
SAC [10]		✓		87.0	41.1	64.0	20.4	12.1	32.8	38.2	47.6	53.1	19.3	81.1	48.9
DACS [45]		✓		86.4	40.0	74.0	27.8	9.5	28.2	71.6	72.0	55.6	20.0	76.4	51.0
PixMatch [73]		✓		90.2	49.9	75.1	23.1	17.4	34.2	67.1	49.9	55.8	14.0	84.3	51.0
DA-VSN [15]	✓			89.4	31.0	77.4	26.1	9.1	20.4	75.4	74.6	42.9	16.1	82.4	49.5
I2VDA [26]		✓		89.9	40.5	77.6	27.3	18.7	23.6	76.1	76.3	48.5	22.4	82.1	53.0
TPS [23]		✓		<u>91.2</u>	<u>53.7</u>	74.9	24.6	17.9	39.3	68.1	59.7	57.2	20.3	84.5	53.8
TPL [25]		✓		90.0	32.8	80.4	28.9	14.9	35.3	80.8	81.1	57.5	19.6	86.7	55.3
DA-STC (Ours)		✓		90.5	41.2	<u>81.1</u>	<u>29.3</u>	<u>23.1</u>	<u>47.5</u>	<u>82.7</u>	<u>83.8</u>	61.1	<u>28.4</u>	<u>87.0</u>	<u>59.6</u>
CMOM* [24]		✓	✓	90.4	39.2	82.3	30.2	16.3	29.6	83.2	84.9	59.3	19.7	84.3	56.3
DA-STC (Ours)*		✓	✓	90.8	39.9	83.2	33.2	30.1	50.7	84.8	82.3	61.2	32.7	87.4	61.5

where \mathcal{G} denotes the video semantic segmentation network, and \mathcal{A} stands for data augmentation. Additionally, X_t represents consecutive image frames, and $o_{t-1 \rightarrow t}$ refers to the corresponding optical flow. Moreover, y_t^S and $\hat{y}_t^{T'}$ are the source label and target pseudo label, respectively, the latter is calculated by Eq. (7), and $\lambda_{\mathcal{T}}$ is the weight decay of target loss. \mathcal{L}_{CE} denotes the cross-entropy loss.

Spatio-temporal feature alignment loss. Furthermore, we map the spatio-temporal aggregated features to the reproducing Hilbert space. By minimizing the mean discrepancy of aggregated source and target domains, we aim to enhance the separation of inter-domain invariant features:

$$\mathcal{L}_{align} = \lambda_f \mathcal{L}_{MMD}(f^S, f^T), \quad (14)$$

where λ_f means the feature loss weight decay.

Self-supervised learning loss. Additionally, we also employ a cross-domain self-supervised learning loss function for both source and target domain videos:

$$\begin{aligned} \mathcal{L}_{SSL} = & \mathcal{L}_{CE}^S(\mathcal{G}(X_t^S, o_{t-1 \rightarrow t}^S), y_t^S) \\ & + \lambda_{\mathcal{T}} \mathcal{L}_{CE}^T(\mathcal{G}(\mathcal{A}(X_t^T), o_{t-1 \rightarrow t}^T), \hat{y}_t^T). \end{aligned} \quad (15)$$

Through self-supervision learning, we exploit the consistency between different fused domains at the spatio-temporal feature level, resulting in a significant reduction of marginal distribution discrepancies between the source and target domain videos. Particularly, the hyperparameter sensitivity for $\lambda_{\mathcal{T}}$ and λ_f will be specifically discussed in the experiments.

IV. EXPERIMENTS

A. Experimental Setups

1) *Datasets and Evaluation Metrics:* In this paper, the experiments are conducted on two challenging benchmarks: SYNTHIA-Seq [29] \rightarrow Cityscapes-Seq [30] and VIPER [31] \rightarrow Cityscapes-Seq, where knowledge from labeled synthetic video generated by game engines are expected to transfer to the real-world unlabeled domain. The Cityscapes-Seq dataset is a standard video semantic segmentation dataset that consists of real city scene videos from 50 cities in Germany and neighboring countries. It comprises 2,975 training video clips and 500 validation video clips, and each clip contains a continuous sequence of 30 frames, with one ground truth label for the 20th frame.

The SYNTHIA-Seq dataset contains 8,000 frames of annotated photo-realistic videos. We use consecutive image frames from the RGB folder as the source domain video dataset, following the same setting as in the literature such as [15] - [24], considering 11 categories for adaptation. The VIPER dataset is another challenging synthetic video dataset, consisting of 133,670 frames of virtual videos rendered from the Grand Theft Auto 5 game engine. We utilize 13,367 frames with labels as another source dataset, choosing 15 categories for adaptation. The resolution of each frame is 1024×2048 , 1080×1920 , and 760×1280 in Cityscapes-Seq, SYNTHIA-Seq, and VIPER respectively. Notably, the data partitioning is consistent with the literature [15], [23], [24], [25], [26].

2) *Implementation Details:* Our model is implemented in PyTorch and trained on a single NVIDIA Tesla V100 GPU. We employ DeepLab-V2 [61] as the video semantic segmentation

TABLE II
 QUANTITATIVE RESULTS IN TERMS OF PER-CATEGORY IOU AND mIOU ON VIPER \rightarrow CITYSCAPES-SEQ. THE BEST RESULT IS HIGHLIGHTED IN BOLD WHILE THE BEST RESULT WITHOUT USING A WARM-UP MODEL IS UNDERLINED. ‘‘Adv.’’: ADVERSARIAL LEARNING, ‘‘SSL’’: SELF-SUPERVISED LEARNING, ‘‘WARM’’: USING A WARM-UP MODEL.

VIPER \rightarrow Cityscapes-Seq																			
Methods	Adv.	SSL	Warm	road	side.	buil.	fenc.	light	sign	vege.	terr.	sky	pers.	car	truc.	bus	mot.	bike	mIOU
Source only	✓			56.7	18.7	78.7	6.0	22.0	15.6	81.6	18.3	80.4	55.9	66.3	4.5	16.8	20.4	10.3	37.1
AdvEnt [65]	✓			78.5	31.0	81.5	22.1	29.2	26.6	81.8	13.7	80.5	58.3	64.0	6.9	38.4	4.6	1.3	41.2
CBST [66]		✓		48.1	20.2	84.8	12.0	20.6	19.2	83.8	18.4	84.9	59.2	71.5	3.2	38.0	23.8	37.7	41.7
IDA [67]	✓			78.7	33.9	82.3	22.7	28.5	26.7	82.5	15.6	79.7	58.1	64.2	6.4	41.2	6.2	3.1	42.0
CRST [68]		✓		56.0	23.1	82.1	11.6	18.7	17.2	85.5	17.5	82.3	60.8	73.6	3.6	38.9	30.5	35.0	42.4
SVMIn [69]				51.1	14.3	80.8	11.9	30.9	23.1	83.5	37.7	74.5	59.5	79.7	36.4	53.2	20.0	4.2	44.1
CrCDA [70]	✓			78.1	33.3	82.2	21.3	29.1	26.8	82.9	28.5	80.7	59.0	73.8	16.5	41.4	7.8	2.5	44.3
RDA [71]		✓		72.0	25.9	80.8	15.1	27.2	20.3	82.6	31.4	82.2	56.3	75.5	22.8	48.3	19.1	6.7	44.4
FDA [72]		✓		70.3	27.7	81.3	17.6	25.8	20.0	83.7	31.3	82.9	57.1	72.2	22.4	49.0	17.2	7.5	44.4
DACS [45]		✓		69.6	24.1	76.9	9.1	16.1	15.3	74.1	20.3	76.5	59.4	74.8	38.6	43.1	7.7	1.9	40.5
SAC [10]		✓		52.2	19.6	73.4	3.7	23.1	25.2	73.9	17.3	78.1	56.9	80.3	38.3	48.2	17.8	14.1	41.5
PixMatch [73]		✓		79.4	26.1	84.6	16.6	28.7	23.0	85.0	30.1	83.7	58.6	75.8	34.2	45.7	16.6	12.4	46.7
DA-VSN [15]	✓			86.8	36.7	83.5	22.9	30.2	27.7	83.6	26.7	80.3	60.0	79.1	20.3	47.2	21.2	11.4	47.8
TPS [23]		✓		82.4	36.9	79.5	9.0	26.3	29.4	78.5	28.2	81.8	61.2	80.2	39.8	40.3	28.5	31.7	48.9
I2VDA [26]		✓		84.8	36.1	84.0	<u>28.0</u>	36.5	36.0	<u>85.9</u>	32.5	74.0	<u>63.2</u>	81.9	33.0	51.8	39.9	0.1	51.2
TPL [25]		✓		89.9	41.5	84.0	7.0	36.5	27.1	85.6	33.7	86.6	62.4	82.6	36.3	47.6	23.2	31.9	51.7
DA-STC (Ours)		✓		<u>91.4</u>	<u>43.5</u>	<u>85.5</u>	21.3	26.6	<u>40.2</u>	84.7	34.2	84.6	62.1	<u>84.3</u>	<u>39.9</u>	46.6	33.5	<u>45.6</u>	54.9
CMOM* [24]		✓	✓	89.0	53.8	86.8	31.0	32.5	47.3	85.6	25.1	80.4	65.1	79.3	21.6	43.4	25.7	40.6	53.8
DA-STC (Ours)*		✓	✓	91.6	51.4	87.0	24.1	32.3	37.2	84.1	28.4	84.8	64.4	85.7	41.4	46.5	34.0	49.6	56.2

network, with ResNet-101 [74] as its backbone pre-trained on ImageNet [75]. In accordance with [15], [23], we employ FlowNet [64] to generate optical flow offline and we set the batch size to 1 due to memory constraint. To facilitate efficient training and inference, we resize the sizes of Cityscapes-Seq, SYNTHIA-Seq, and VIPER to 1024×512 , 760×1280 , and 720×1280 , respectively, using bilinear interpolation. All models are trained using the SGD optimizer with a momentum of 0.9 and a weight decay of 5×10^{-4} . For target domain videos, we apply Gaussian blur and color jitter for data augmentation. The initial learning rate is set to 2.5×10^{-4} for SYNTHIA-Seq to Cityscapes-Seq, and 1×10^{-4} for VIPER to Cityscapes-Seq. On both datasets, the model is trained for a maximum of 40,000 iterations. Consistent with [15] - [24], we use a cross frame interval τ of 1. Additionally, the confidence threshold γ for the target domain sequence templates is set to 0.9. In the process of constructing the two fused domains, source domain frames undergo random cropping to match the dimensions of the target frames. The widely used per-category IOU and average mIOU are used as the evaluation metrics in this paper.

Moreover, it has been noticed that the models always exhibit low or even zero segmentation IOU on certain categories [76], [45]. Apart from the domain gap, we attribute this to the long-tail effect. Therefore, we also perform BSTF and category-aware feature alignment for long-tail categories similarly. We choose *fence*, *pole*, *light*, *sign*, and *rider* for the SYNTHIA-Seq adaptation task, and *fence*, *light*, *sign*, *terrain*, *motor*, and *bike* for the VIPER adaptation task.

B. Comparison With State-of-the-Art Methods

As shown in Table I and Table II, we compare our proposed DA-STC method with the state-of-the-art methods on the VIPER \rightarrow Cityscapes-Seq and SYNTHIA-Seq \rightarrow Cityscapes-Seq benchmarks. To the best of our knowledge, DA-VSN [15], TPS [23], I2VDA [26], TPL [25], and CMOM [24] stand as recent contributions in the emerging field of DAVSS, which has recently gained substantial attention. Additionally, we compare our method with several customized baselines originally designed for domain adaptation in image segmentation, including AdvEnt [65], CBST [66], IDA [67], CRST [68], SVMIn [69], CrCDA [70], RDA [71], FDA [72], SAC [10], DACS [45], and PixMatch [73]. The variants of these baselines follow the same approach as in [23] - [24] by just replacing the image segmentation backbone with the video segmentation network to achieve video domain adaptation. In the notation used, ‘‘Adv.’’ signifies methods that employ adversarial learning, ‘‘ST’’ denotes methods leveraging self-supervised learning, and ‘‘Warm’’ indicates that the model is trained stagewise with a warm-up model, while other methods are initialized with parameters pre-trained on ImageNet using ResNet-101. They are particularly indicated by the symbol * in the last two rows of Table I and Table II.

Synthia-Seq \rightarrow Cityscapes-Seq. In Table I, we present the experimental results of the proposed DA-STC method and state-of-the-art methods on the Synthia-Seq \rightarrow Cityscapes-Seq benchmark. For a fair comparison, the best per-category IOU and mIOU for methods without using a warm-up model are underlined, while the best IOU and mIOU for all methods are in bold. We observed that: (i) the proposed DA-STC method

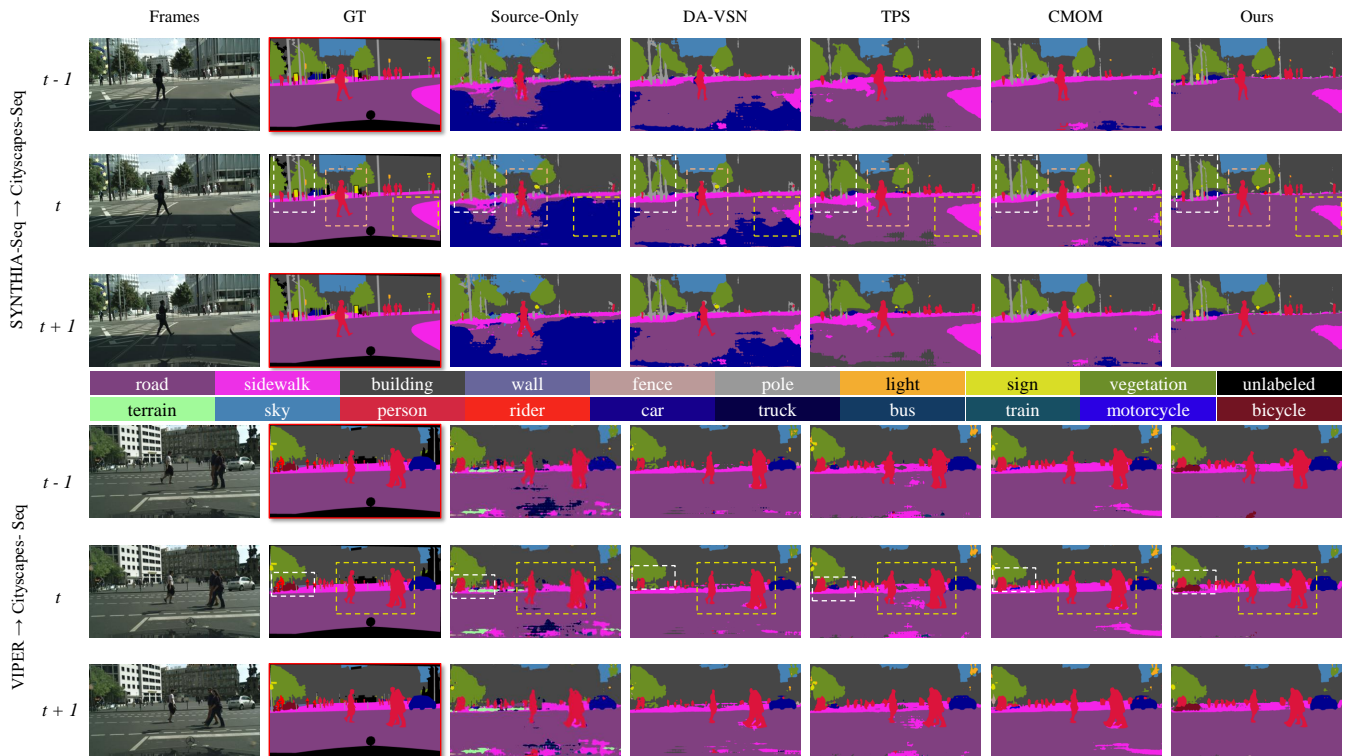


Fig. 6. Qualitative results for consecutive three frames from Cityscapes (Val). The results are presented in the following order: target image, ground truth, predictions from Source Only, DA-VSN [15], TPS [23], CMOM [24], and our method. Each result is displayed from left to right. Our method demonstrates a noticeable visual enhancement. Best viewed in color.

significantly outperforms the source-only model with a 38.3% mIOU; (ii) our method initialized with ImageNet pre-trained parameters achieved 59.6% mIOU, which is 4.3% higher than the second-best TPL method [25] with a large margin. Notably, it is also 3.3% higher than the CMOM model [24] that depends heavily on the warm-up model. In CMOM, both initial model parameters and pseudo labels are obtained exclusively based on the pre-trained model. By contrast, when we only initialize the parameters with the warm-up model, our mIOU can be further improved by 1.9%, reaching the highest 61.5%; (iii) adversarial learning methods can improve the model’s transferability, but the effect is not as pronounced as self-supervised methods; (iv) our method significantly improves the IOU of long-tail categories and achieves the best performance on the selected long-tail categories. The improvement can be attributed to our additional attention to the spatio-temporal information of long-tail categories within the BSTF module, as well as cross-domain alignment for multiple aggregated subdomain features.

Viper → Cityscapes-Seq. As shown in Table II, the proposed DA-STC also achieves superior results on Viper → Cityscapes-Seq. We can conclude that: (i) our method achieves 56.2% mIOU with a warm-up model and achieves 54.9% mIoU only using the ImageNet pre-trained parameters for initialization, outperforming the source-only model by 19.1% and 17.8% respectively; (ii) our method achieves the highest IOU of 49.6% for the long-tail category *bike*, while some other methods exhibit lower or even close-to-zero metrics.

This underscores the effectiveness of our method on hard-to-transfer categories; (iii) it is worth noting that the variations of image domain adaptation methods tend to underperform in target videos compared to DAVSS methods. This disparity is speculated to arise from the emphasis on spatial features while overlooking the utilization of temporal information; (iv) the recent work I2VDA [26] exclusively focuses on the transfer of source spatial information to target domain videos, resulting in a target domain mIOU of 51.7%, which is inferior to our model of 56.2% that considers both spatial and temporal information simultaneously.

Qualitative results comparison on two benchmarks. In Fig. 6, we present image sequences from the target validation set for two synthetic-to-real video benchmarks, along with the label of the t -th frame. The Cityscape-Seq dataset [30] provides a label only for the 19th frame of each video clip containing 30 frames due to laborious annotation. Therefore, we display the same label for frames $t - 1$ and $t + 1$, distinguished by red borders for reference. We present the qualitative results of our method along with the source-only model, DA-VSN [15], TPS [23], and CMOM [24]. The segmentation maps of our method exhibit smoother edges and finer details. For instance, in the SYNTHIA-Seq → Cityscapes-Seq benchmark, we achieve more accurate segmentation for categories like person, sign, and sidewalk. Similarly, in the case of Viper → Cityscapes-Seq, our model predicts contours that closely resemble actual bicycles and persons, indicating a significant enhancement for target-domain videos.

TABLE III

ABLATION STUDY OF mIOU (%) ON SYNTHIA-SEQ \rightarrow CITYSCAPES-SEQ. ALL MODELS ARE TRAINED END-TO-END FOR A TOTAL OF 40K ITERATIONS. IN THIS TABLE, “I-TMPL” INDICATES BIDIRECTIONAL FUSION WITH JUST A SINGLE IMAGE TEMPLATE LIKE [27], WHILE “S-TMPL” REPRESENTS OUR FUSION STRATEGY AT IMAGE SEQUENCE TEMPLATE LEVEL AND OPTICAL FLOW LEVEL. “FEAT-F” DENOTES THE SHALLOW FEATURE-LEVEL FUSION, “LT” SIGNIFIES THE CONSIDERATION OF LONG-TAIL CATEGORIES IN BSTF, AND “ALIGN” REFERS TO THE CATEGORY-AWARE SPATIO-TEMPORAL FEATURE ALIGNMENT MODULE.

Exp.	SSL	I-tmpl	S-tmpl	Feat-F	LT	Align	Warm	mIOU / $\Delta \uparrow$
1	✓							52.01 / -
2	✓	✓						55.43 / 3.42
3	✓		✓					55.71 / 3.70
4	✓		✓	✓				56.25 / 4.24
5	✓		✓	✓	✓			57.55 / 5.54
6	✓		✓	✓	✓		✓	57.95 / 5.95
7	✓					✓		54.01 / 2.00
8	✓		✓	✓	✓	✓		<u>59.62 / 7.61</u>
9	✓		✓	✓	✓	✓	✓	61.48 / 9.47

C. Ablation Study

The effect of each module. Table III presents the ablation results for each module. Exp. 5 and Exp. 7 correspond to the two proposed modules, while Exp. 9 denotes the comprehensive result. For a fair comparison, we take the results of TPS [23] without random scale augmentation as the baseline (Exp. 1). It is observed that Exp. 2 and 3 improved over Exp. 1 by 3.42% and 3.70% respectively, indicating that constructing fused intermediate domains could enhance the transfer learning capacity of the model. We attribute this to the distinct spatio-temporal contexts of two fused domains, which helps to learn robust spatio-temporal features of shared patch sequences. The mIOU scores of Exp. 3 are higher than Exp. 2, suggesting that sequence templates are more conducive compared to only image templates. Moreover, in Exp. 4, feature fusion is conducted in two fused intermediate domains, resulting in improved model performance. Exp. 5 takes a step further by considering long-tail categories when constructing bidirectional templates, leading to an additional increase to 56.25%.

Furthermore, Exp. 7 introduces the feature alignment module based on Exp. 1, resulting in an improvement to 54.01%, highlighting the effectiveness of the category-aware spatio-temporal feature alignment module across two domains. Exp. 8 combines the BSTF and Align modules, achieving a performance of 59.62% without requiring a warm-up model, surpassing the state-of-the-art TPL [25] mIOU of 55.3% by 4.32%. Moreover, we also employ the warm-up setup in Exp. 6 and Exp. 9 for parameter initialization, both exceeding the state-of-the-art CMOM of 56.31% with a warm-up stage. It is noteworthy that Exp. 6 only includes the BSTF module, and Exp. 9 further introduces the feature alignment module, resulting in the highest mIOU of 61.48%, a remarkable 9.47% increase compared to the baseline. The above analyses collectively validate the effectiveness of the proposed modules and the idea of exploiting the consistency in learning cross-domain

TABLE IV

ABLATION STUDY OF THE NUMBER OF LONG-TAIL (LT) SOURCE CATEGORIES ON SYNTHIA-SEQ \rightarrow CITYSCAPES-SEQ.

Number of LT categories (K^S)	0	1	2	3	4
mIOU(%)	59.87	59.31	61.48	60.29	60.72

TABLE V

ABLATION STUDY OF THE BIDIRECTIONAL FUSION CATEGORY SPACES ON SYNTHIA-SEQ \rightarrow CITYSCAPES-SEQ.

Fusion categories	Things	Stuffs	Movable	Stationary	All
mIOU(%)	58.53	57.50	58.29	55.55	61.48

invariant features.

Qualitative results of each module. In Fig. 7, taking SYNTHIA-Seq \rightarrow Cityscapes-Seq as an example, we present segmentation maps for three consecutive frames with different configurations. The qualitative outcomes align with the expectations derived from Table III. As we observe from left to right, the models steadily improve the accuracy of segments such as person and sign. Notably, the buses at the far right within the images present a challenging prediction scenario, which is effectively addressed by the combined approach of multiple modules (Exp. 9). The progressive left-to-right results illustrate the cumulative influence of module integration.

The effect of long-tail categories used for fusion. Table III has shown the benefits of focusing on source long-tail category patches. Thus, we initiate ablation experiments by varying the number of randomly selected categories from the long-tail category space K^S . As illustrated in Table IV, using SYNTHIA-Seq \rightarrow Cityscapes-Seq as an example, when the number of long-tail categories \tilde{n} is 2, the mIOU metric is highest. Compared with $\tilde{n} = 0$, there are also notable improvements when \tilde{n} is set to 3 or 4. However, when \tilde{n} is reduced to 1, a slight decrease is observed. We suggest that this might be ascribed to the limited semantic information contained within small pixel templates of a single category, a tendency that diminishes as the category number increases.

The effect of fusion category spaces for K^S and K^T . The templates in the two fused intermediate domains encompass information corresponding to both the source category space K^S and the target category space K^T . Additionally, bidirectional templates from two domains incorporate the semantics of two categories respectively that are mutually exclusive. We investigated the impact of the category space on model performance. Things (e.g., signs, cars) and stuffs (e.g., sky, road) are common category divisions in panoramic segmentation [77]. In Table V, we explored the model performance when the fused category comprised exclusively of things or stuff. Additionally, we further conducted ablation experiments where the fused category space encompassing solely movable (e.g., persons, cars) or stationary (e.g., signs, lights) objects [24]. The experimental results indicate that things and movable categories hold greater significance, and interestingly, the model achieves the best performance when the fused category space includes all categories. This finding underscores the versatility of our

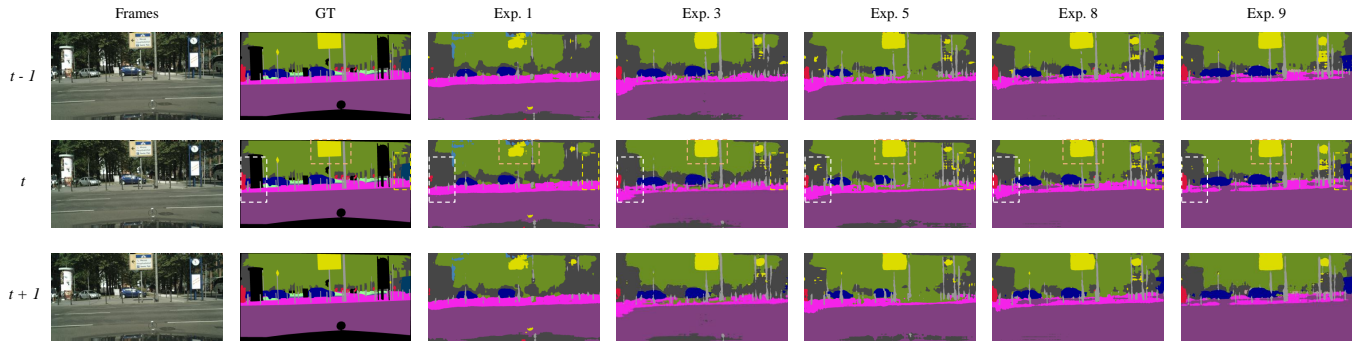


Fig. 7. Qualitative outputs with module integration for three consecutive frames on SYNTHIA-Seq \rightarrow Cityscapes-Seq. The best results are achieved with the rightmost module combination (Exp. 9), especially for categories such as person, rider, and car. Best viewed in color.

TABLE VI

ABLATION STUDY RESULTS OF mIOU (%) ON THE CONSTRUCTION OF INTERMEDIATE DOMAINS AND TEMPLATES ON SYNTHIA-SEQ \rightarrow CITYSCAPES-SEQ.

	Source tmlp	Target tmlp	Source & Target tmlp
only $X_t^{S'}$	60.49	57.84	59.55
only $X_t^{T'}$	58.38	56.67	58.39
both $X_t^{S'}$ and $X_t^{T'}$	60.40	59.39	61.48

TABLE VII

ABLATION STUDY RESULTS OF mIOU (%) ON AUGMENTATION OF TARGET INPUTS AND CROSS-DOMAIN CATEGORY-AWARE SPATIO-TEMPORAL FEATURE ALIGNMENT.

Method	SYN-Seq \rightarrow City-Seq	VIPER \rightarrow Cityscapes-Seq
w/o aug	60.23	55.25
w/aug	61.48 (\uparrow 1.25)	56.16 (\uparrow 0.91)
global feature align	58.24	53.62
category-aware feature align	61.48 (\uparrow 3.24)	56.16 (\uparrow 2.54)

BSTF module across categories and its profound impact on enhancing the model’s adaptation to target domain videos.

The effect of construction method for intermediate domains. In Section III-C, we generate random category-aware sequence templates from both the source and target domains, which are then bidirectionally fused into the source and target domains at multiple levels: input, optical flow, and label levels, along with feature fusion for the two intermediate domains. This naturally prompts us to explore the outcomes when templates are exclusively from the source or target domain, or when only the fused source or target domain is constructed. The experimental results for these scenarios are provided in Table VI.

It can be observed: (i) vertically, the construction of bidirectional fused domains often yields better outcomes in comparison to creating a sole fused domain [45], [24]. This is because the model can learn richer spatio-temporal features across domains, with the feature-level fusion of intermediate domains also serving as a supportive factor; (ii) horizontally, utilizing source domain templates with labels outperforms using target

TABLE VIII

ABLATION STUDY OF LOSS WEIGHTS ON VIPER \rightarrow CITYSCAPES-SEQ.

Weights	mIoU(%)
$\lambda_{\mathcal{T}}, \lambda_f = 0.10, 0.01$	54.56
$\lambda_{\mathcal{T}}, \lambda_f = 0.20, 0.01$	56.16
$\lambda_{\mathcal{T}}, \lambda_f = 0.50, 0.01$	54.49
$\lambda_{\mathcal{T}}, \lambda_f = 0.50, 0.10$	54.56
$\lambda_{\mathcal{T}}, \lambda_f = 0.70, 0.10$	54.58
$\lambda_{\mathcal{T}}, \lambda_f = 1.00, 0.10$	<u>55.20</u>

domain templates with higher predictive confidence. The overall mIOU exhibits further improvement when incorporating templates from both domains, particularly pronounced when constructing two fused domains, achieving a peak mIOU of 61.48%; (iii) comprehensively, the benefit of incorporating the source target domain is more significant than that of a only fused target domain, it is an intriguing phenomenon that has been overlooked by prior works [24], [27], [45]. We find that the construction of fused source domains serves as an effective augmentation strategy, significantly improving the model’s generalization. Furthermore, the results validate the benefit of creating two fused intermediate domains, leading to a performance increase from 58.39% to 61.48%.

It’s worth noting that regardless of the mixing strategy adopted, the performance in Table VI all surpasses previous state-of-the-art methods CMOM [24] and TPL [25], demonstrating the effectiveness of our method.

The effect of category-aware feature alignment and target augmentation. Prior studies [27] implicitly align spatial feature distributions by minimizing domain discrepancy. By exclusively substituting the proposed alignment module with prior methods, we achieved mIOUs of 58.24% and 53.62% on two benchmarks respectively, as shown in Table VII. Notably, our category-aware spatio-temporal feature alignment outperforms this implicit method by 3.24% and 2.54%, underscoring its efficacy in aligning feature distributions across category subspaces. In Table VII, we also investigate the advantage of target domain data augmentation \mathcal{A} in Eq. (13) and Eq. (15).

TABLE IX

ABLATION STUDY RESULTS OF mIOU (%) ON MODEL INITIALIZATION. THE “ORIGINAL” COLUMN DENOTES THE RESULTS FROM THE ORIGINAL PAPERS, AND THE “DA-STC” COLUMN REPRESENTS THE RESULTS OF OUR MODELS INITIALIZED WITH WARM-UP MODELS FROM THE WORKS IN “ORIGINAL” COLUMN, RESPECTIVELY.

Method	SYN-Seq → City-Seq		VIPER → City-Seq	
	Original	DA-STC	Original	DA-STC
ResNet-101 [74]	32.01	59.62	24.60	54.94
DA-VSN [15]	49.53	59.07	47.84	55.31
CMOM [24]	56.31	60.33	53.81	56.10
TPS [23]	53.76	61.48	48.91	56.16

TABLE X

THROUGHPUT MEASURED FOR DIFFERENT MODULES. RESULTS ARE OBTAINED USING V100-32G AND THROUGHPUT IS MEASURED USING A BATCH SIZE OF 1.

Modules	SYN-Seq → City-Seq		VIPER → City-Seq	
	Training time (s/iter)	Memory	Training time (s/iter)	Memory
Src.	1.40	8990M	1.38	8990M
SSL	2.31	12822M	2.34	13872M
BSTF	3.78	21750M	3.99	22426M
Align	4.26	25514M	4.37	26524M

D. Further Analysis

1) *Hyperparameter Sensitivity*: In terms of model optimization, we utilize two hyperparameters, $\lambda_{\mathcal{T}}$ in Eq. (13) and Eq. (15) as the weight for self-supervised target loss, and λ_f in Eq. (14) for category-aware feature consistency loss across domains. The weight of the source loss is set to 1. In Table VIII, we progressively increase the values of $\lambda_{\mathcal{T}}$ and λ_f using Viper → Cityscapes-Seq as an example to explore the influence of different parameter settings. The model achieves an mIOU of 56.16% with these parameters set to 0.20 and 0.01, and a suboptimal mIOU of 55.20% when the two parameters are set to 1.00 and 0.10. The performance displays slight fluctuations with changes in parameter settings, showing the robustness of our method. Similarly, we set $\lambda_{\mathcal{T}}$ and λ_f to be equal to 1 on Synthea-Seq → Cityscapes-Seq.

2) *Results with Different Model Initialization*: End-to-end [48] and staged training [12] are two paradigms in domain adaptation research. In semantic segmentation, the former usually initialize model parameters with those pre-trained on ImageNet using ResNet-101, while parameters of the latter often build upon a warm-up model. We investigated the impact of model initialization on performance. As shown in Table IX, our model achieved an mIOU of 59.62% and 54.94% on the two benchmarks respectively via end-to-end training. Initializing our model with various warm-up models from previous works in the “Original” column can also enhance the performance by a large margin compared with previous DAVSS methods. Notably, the recent advanced method CMOM [24] employs a multi-stage training approach and generates initial pseudo labels using a warm-up model

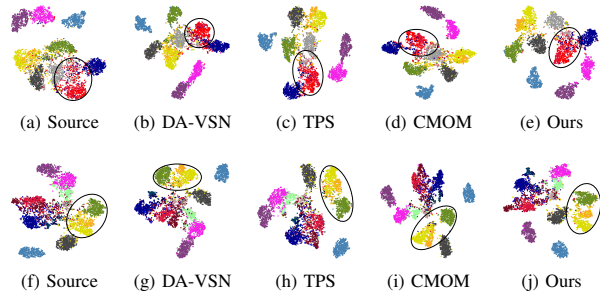


Fig. 8. T-SNE analysis of existing methods and ours on SYNTHIA-Seq → Cityscapes-Seq (first line) and VIPER → Cityscapes-Seq (second line). Our model excels in learning discriminative features of target videos in embedding space. Please zoom in to view.

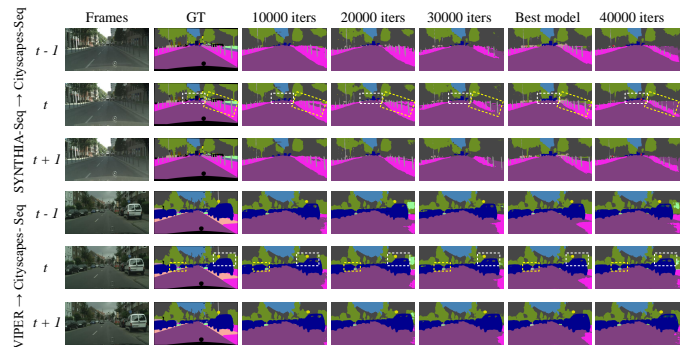


Fig. 9. Qualitative results of our model across different training iterations as well as the best model for two benchmarks.

trained in [15]. In contrast, our model solely undergoes model initialization. According to Table IX, whether utilizing an end-to-end or staged training paradigm, our method outperforms the previous state-of-the-art CMOM [24] on two benchmarks. These experiments underscore the remarkable adaptation capacity of our model on target domain videos.

3) *The throughput Measured for Different Modules*: The primary innovation of our approach lies in the two novel modules, and the combination of cross-frame generation for target pseudo labels. In Table X, we present the training time and GPU memory footprint associated with the utilization of different modules. “Src.” refers to training only with the source domain data. Compared to using only the self-supervised learning (SSL) loss as [23], the inclusion of the BSTF module leads to a modest increase in training time and GPU memory, whereas “Align” exhibits relatively lighter overhead. Notably, as shown in part (c) of Fig. 2, during model testing, only adjacent frames and optical flow are required as inputs. In line with [15], [23], [24], [25], our method maintains similar inference speed and memory footprint.

4) *T-SNE Analysis of Existing Methods and Ours*: For better visualization, we generated t-SNE visualizations of the embedding vectors obtained from three recent methods and the source-only model. They are compared with our DA-STC method, as depicted in Fig. 8. The categories corresponding to each color of the dots are consistent with Fig. 6. We could observe that the category-wise clusters of recent methods tend to be more dispersed in terms of inter-category discrimina-

TABLE XI
 QUANTITATIVE RESULTS IN TERMS OF PER-CATEGORY IOU AND mIOU FOR IMAGE DOMAIN ADAPTIVE SEMANTIC SEGMENTATION TASK ON GTAV \rightarrow CITYSCAPES. THE BEST RESULTS ARE HIGHLIGHTED IN BOLD.

GTAV \rightarrow Cityscapes																				
Methods	road	side.	buil.	wall	fence	pole	light	sign	vege.	terr.	sky	pers.	rider	car	truck	bus	train	moto.	bike	mIOU
Source Only	63.3	15.7	59.4	8.6	15.2	18.3	26.9	15.0	80.5	15.3	73.0	51.0	17.7	59.7	28.2	33.1	3.5	23.2	16.7	32.9
AdvEnt [65]	89.4	33.1	81.0	26.6	26.8	27.2	33.5	24.7	83.9	36.7	78.8	58.7	30.5	84.8	38.5	44.5	1.70	31.6	32.4	45.5
CAG-UDA [56]	90.4	51.6	83.8	34.2	27.8	38.4	25.3	48.4	85.4	38.2	78.1	58.6	34.6	84.7	21.9	42.7	41.1	29.3	37.2	50.2
CRCDA [70]	92.4	55.3	82.3	31.2	29.1	32.5	33.2	35.6	83.5	34.8	84.2	58.9	32.2	84.7	40.6	46.1	2.10	31.1	32.7	48.6
FDA [72]	92.5	53.3	82.4	26.5	27.6	36.4	40.6	38.9	82.3	39.8	78.0	62.6	34.4	84.9	34.1	53.1	16.9	27.7	46.4	50.5
PixMatch [73]	91.6	51.2	84.7	37.3	29.1	24.6	31.3	37.2	86.5	44.3	85.3	62.8	22.6	87.6	38.9	52.3	0.70	37.2	50.0	50.3
RDA [71]	93.1	55.0	84.7	33.1	29.5	38.7	49.3	44.9	84.8	41.6	80.2	62.3	33.2	85.6	37.3	51.3	18.5	34.6	45.3	52.8
SAC [10]	90.4	53.9	86.6	42.4	27.3	45.1	48.5	42.7	87.4	40.1	86.1	67.5	29.7	88.5	49.1	54.6	9.80	26.6	45.3	53.8
DACS [45]	89.9	39.7	87.9	39.7	39.5	38.5	46.4	52.8	88.0	44.0	88.8	67.2	35.8	84.5	45.7	50.2	0.00	27.3	34.0	52.1
DSP [27]	92.4	48.0	87.4	33.4	35.1	36.4	41.6	46.0	87.7	43.2	89.8	66.6	32.1	89.9	57.0	56.1	0.00	44.1	57.8	55.0
I2F [78]	90.8	48.7	85.2	30.6	28.0	33.3	46.4	40.0	85.6	39.1	88.1	61.8	35.0	86.7	46.3	55.6	11.6	44.7	54.3	53.3
DA-SC (Ours)	92.9	52.6	87.8	35.9	39.0	33.7	42.1	54.4	87.8	42.9	91.2	66.9	26.7	90.3	65.0	59.3	0.10	38.3	58.9	56.1

tion, whereas our method is more concentrated. For instance, categories like perdon, rider, and fence in SYNTHIA-Seq \rightarrow Cityscapes-Seq, as well as categories like light, sign, and vegetation in VIPER \rightarrow Cityscapes-Seq, exhibit more compact intra-category space and more distinct inter-category differences in our method, revealing the discriminative capability towards various categories in the target domain.

5) *Results of Different Training Iterations:* In Fig. 9, we provide a more comprehensive presentation of the visual results of semantic segmentation for models trained at different iterations. Notably, the best models for both benchmarks emerge between the 30k and 40k iterations, providing a clearer insight into the evolution and stability of the model training process.

E. Extended Application to Image Domain

The above sections illustrate the effectiveness of our DA-STC method for adapting to unlabeled video target domains. To assess its generality, we introduce a variant called DA-SC for image domain adaptation, which is achieved by simply replacing the spatio-temporal consistency with spatial consistency across two domains. Specifically, we shift our focus from image pairs $X_t = \{x_{t-1}, x_t\}$ to a single image x , remove the optical flow information, and aggregate only spatial features for feature alignment. Additionally, we generate target pseudo labels using a momentum network [79]. Through these modifications, we expand the scope of our method to image domain adaptation tasks.

1) *Datasets and Implementation Details:* GTAV is a synthetic image dataset with labels for semantic segmentation, where images are derived from urban landscape scenes in the virtual computer game ‘‘Grand Theft Auto V.’’ This dataset comprises 19 categories and 24,966 labeled images with a resolution of 1914×1052 . The Cityscapes dataset is a subset of Cityscapes-Seq, with each image being the 20th frame of the corresponding video clip. Following prior works, we employ unlabeled Cityscapes as the target domain, and the GTAV dataset as the source domain. The experimental

setup aligns with previous works [45], [27], and we employ DeepLabv2 [61] with a ResNet101 backbone pre-trained on ImageNet MSCOCO [80] as the network. We utilize SGD optimizer with an initial learning rate of 2.5×10^{-4} , weight decay of 5×10^{-4} , and a momentum of 0.9. The batch size is set to 2, and the training iterations are 250k. Data from both domains undergo resizing to dimensions of 760×1280 and 512×1024 , followed by random cropping to a final size of 512×512 . We set λ_{τ} and λ_f to be equal to 1.

2) *Comparison With Existing Methods:* In Table XI, we present quantitative comparisons of our variant DA-SC with existing methods using Deeplabv2-ResNet101 for image domain adaptive semantic segmentation, highlighting the best results in bold. Impressively, our method maintains its superiority on the GTAV \rightarrow Cityscapes benchmark, achieving a remarkable mIOU of 56.1%, a significant improvement over the baseline model trained solely with source domain data, which attains a mere 33.1%. Notably, our method outperforms recent methods like I2F [78], DACS [45], and DSP [27]. I2F focuses on global photometric and texture alignment, and the latter two generate enhanced target images only with well-labeled source domain patches, while overlooking the target domain templates with high confidence, as well as the shallow feature-level fusion. These experimental results emphasize the effectiveness of our proposed modules, including bidirectional multiple-level fusion module and category-aware feature alignment. Overall, the experiments demonstrate our method’s capacity to effectively extend to image domain adaptation scenarios.

V. CONCLUSION

This paper proposes DA-STC, a self-supervised learning method tailored for domain adaptive video semantic segmentation. It significantly improves the transfer capability of models on unlabeled target domain videos characterized by substantial domain shifts. Our main innovations include a bidirectional spatio-temporal fusion module at the input level, feature level, and label level, as well as a category-aware spatio-temporal feature alignment module. They help the model to

learn robust features from category-aware patch sequences shared between two intermediate domains with distinct spatio-temporal contexts, and perform cross-domain spatio-temporal feature alignment in category subdomains to improve cross-domain consistency learning. Additionally, we address the emphasis on learning long-tail categories. Our approach is comprehensive and effective, demonstrating surprising effectiveness. Extensive experiments confirm the superiority of the DA-STC method on two challenging domain adaptive video semantic segmentation benchmarks, as well as the extended application to image domain adaptation scenarios.

ACKNOWLEDGMENT

This work was supported in part by the Major Program of National Natural Science Foundation of China (NSFC) under Grant 61991400, and 61991404, in part by the NSFC under Grants 62103092. The authors appreciate Lan Deng for suggestions. Zhe Zhang expresses gratitude to Xiaojuan Zhang for the companionship and support.

REFERENCES

- [1] K. Muhammad, T. Hussain, H. Ullah, J. Del Ser, M. Rezaei, N. Kumar, M. Hijji, P. Bellavista, and V. H. C. de Albuquerque, "Vision-based semantic segmentation in scene understanding for autonomous driving: Recent achievements, challenges, and outlooks," *IEEE Trans. Intell. Transp. Syst.*, vol. 23, no. 12, pp. 22 694–22 715, 2022.
- [2] Mo, Yujian, Wu, Yan, Yang, Xinneng, Liu, Feilin, and Liao, Yujun, "Review the state-of-the-art technologies of semantic segmentation based on deep learning," *Neurocomputing*, vol. 493, pp. 626–646, 2022.
- [3] Gupta Deepak, Attal Kush, and Demner-Fushman Dina, "A dataset for medical instructional video classification and question answering," *Sci. Data*, vol. 10, no. 1, pp. 1–16, 2023.
- [4] S. Wan, X. Xu, T. Wang, and Z. Gu, "An intelligent video analysis method for abnormal event detection in intelligent transportation systems," *IEEE Trans. Intell. Transp. Syst.*, vol. 22, no. 7, pp. 4487–4495, 2020.
- [5] Y. Zhang, T. Liu, M. Long, and M. Jordan, "Bridging theory and algorithm for domain adaptation," in *Proc. Int. Conf. Mach. Learn.*, 2019, pp. 7404–7413.
- [6] Y. Luo, L. Zheng, T. Guan, J. Yu, and Y. Yang, "Taking a closer look at domain shift: Category-level adversaries for semantics consistent domain adaptation," in *Proc. IEEE Conf. Comput. Vis. Pattern Recognit.*, 2019, pp. 2507–2516.
- [7] J. Hoffman, E. Tzeng, T. Park, J.-Y. Zhu, P. Isola, K. Saenko, A. Efros, and T. Darrell, "Cycada: Cycle-consistent adversarial domain adaptation," in *Proc. Int. Conf. Mach. Learn.*, 2018, pp. 1989–1998.
- [8] Y. Zhang, H. Tang, K. Jia, and M. Tan, "Domain-symmetric networks for adversarial domain adaptation," in *Proc. IEEE Conf. Comput. Vis. Pattern Recognit.*, 2019, pp. 5031–5040.
- [9] M. Long, Z. Cao, J. Wang, and M. I. Jordan, "Conditional adversarial domain adaptation," in *Proc. Adv. Neural Inf. Process. Syst.*, 2018, pp. 1647–1657.
- [10] N. Araslanov and S. Roth, "Self-supervised augmentation consistency for adapting semantic segmentation," in *Proc. IEEE Conf. Comput. Vis. Pattern Recognit.*, 2021, pp. 15 384–15 394.
- [11] T. Isobe, X. Jia, S. Chen, J. He, Y. Shi, J. Liu, H. Lu, and S. Wang, "Multi-target domain adaptation with collaborative consistency learning," in *Proc. IEEE Conf. Comput. Vis. Pattern Recognit.*, 2021, pp. 8187–8196.
- [12] P. Zhang, B. Zhang, T. Zhang, D. Chen, Y. Wang, and F. Wen, "Prototypical pseudo label denoising and target structure learning for domain adaptive semantic segmentation," in *Proc. IEEE Conf. Comput. Vis. Pattern Recognit.*, 2021, pp. 12 414–12 424.
- [13] A. Gretton, K. M. Borgwardt, M. J. Rasch, B. Schölkopf, and A. Smola, "A kernel two-sample test," *J. Mach. Learn. Res.*, vol. 13, no. 1, pp. 723–773, 2012.
- [14] B. Sun and K. Saenko, "Deep coral: Correlation alignment for deep domain adaptation," in *Proc. Eur. Conf. Comput. Vis.*, 2016, pp. 443–450.
- [15] D. Guan, J. Huang, A. Xiao, and S. Lu, "Domain adaptive video segmentation via temporal consistency regularization," in *Proc. IEEE Int. Conf. Comput. Vis.*, 2021, pp. 8053–8064.
- [16] P. Hu, F. Caba, O. Wang, Z. Lin, S. Sclaroff, and F. Perazzi, "Temporally distributed networks for fast video semantic segmentation," in *Proc. IEEE Conf. Comput. Vis. Pattern Recognit.*, 2020, pp. 8818–8827.
- [17] Z. Yang and Y. Yang, "Decoupling features in hierarchical propagation for video object segmentation," in *Proc. Adv. Neural Inf. Process. Syst.*, 2022, pp. 36 324–36 336.
- [18] L. Ru, Y. Zhan, B. Yu, and B. Du, "Learning affinity from attention: End-to-end weakly-supervised semantic segmentation with transformers," in *Proc. IEEE Conf. Comput. Vis. Pattern Recognit.*, 2022, pp. 16 846–16 855.
- [19] Y. Li, J. Shi, and D. Lin, "Low-latency video semantic segmentation," in *Proc. IEEE Conf. Comput. Vis. Pattern Recognit.*, 2018, pp. 5997–6005.
- [20] X. Song, S. Zhao, J. Yang, H. Yue, P. Xu, R. Hu, and H. Chai, "Spatio-temporal contrastive domain adaptation for action recognition," in *Proc. IEEE Conf. Comput. Vis. Pattern Recognit.*, 2021, pp. 9787–9795.
- [21] H. Coskun, M. Z. Zia, B. Tekin, F. Bogo, N. Navab, F. Tombari, and H. Sawhney, "Domain-specific priors and meta learning for few-shot first-person action recognition," *IEEE Trans. Pattern Anal. Mach. Intell.*, vol. 45, no. 6, pp. 6659–6673, 2023.
- [22] Y. Xu, H. Cao, K. Mao, Z. Chen, L. Xie, and J. Yang, "Aligning correlation information for domain adaptation in action recognition," *IEEE Trans. Neural Netw. Learn. Syst.*, pp. 1–12, 2022.
- [23] Y. Xing, D. Guan, J. Huang, and S. Lu, "Domain adaptive video segmentation via temporal pseudo supervision," in *Proc. Eur. Conf. Comput. Vis.*, 2022, pp. 621–639.
- [24] K. Cho, S. Lee, H. Seong, and E. Kim, "Domain adaptive video semantic segmentation via cross-domain moving object mixing," in *Proc. IEEE Winter Conf. Appl. Comput. Vis.*, 2023, pp. 489–498.
- [25] Y. Gao, Z. Wang, J. Zhuang, Y. Zhang, and J. Li, "Exploit domain-robust optical flow in domain adaptive video semantic segmentation," in *Proc. AAAI Conf. Artif. Intell.*, 2023, pp. 641–649.
- [26] X. Wu, Z. Wu, J. Wan, L. Ju, and S. Wang, "Is it necessary to transfer temporal knowledge for domain adaptive video semantic segmentation?" in *Proc. Eur. Conf. Comput. Vis.*, 2022, pp. 357–373.
- [27] L. Gao, J. Zhang, L. Zhang, and D. Tao, "Dsp: Dual soft-paste for unsupervised domain adaptive semantic segmentation," in *Proc. ACM Int. Conf. Multimed.*, 2021, pp. 2825–2833.
- [28] Q. Zhou, Q. Gu, J. Pang, X. Lu, and L. Ma, "Self-adversarial disentangling for specific domain adaptation," *IEEE Trans. Pattern Anal. Mach. Intell.*, vol. 45, no. 7, pp. 8954–8968, 2023.
- [29] G. Ros, L. Sellart, J. Materzynska, D. Vazquez, and A. M. Lopez, "The synthia dataset: A large collection of synthetic images for semantic segmentation of urban scenes," in *Proc. IEEE Conf. Comput. Vis. Pattern Recognit.*, 2016, pp. 3234–3243.
- [30] M. Cordts, M. Omran, S. Ramos, T. Rehfeld, M. Enzweiler, R. Benenson, U. Franke, S. Roth, and B. Schiele, "The cityscapes dataset for semantic urban scene understanding," in *Proc. IEEE Conf. Comput. Vis. Pattern Recognit.*, 2016, pp. 3213–3223.
- [31] S. R. Richter, Z. Hayder, and V. Koltun, "Playing for benchmarks," in *Proc. IEEE Int. Conf. Comput. Vis.*, 2017, pp. 2213–2222.
- [32] S. K. Panda, Y. Lee, and M. K. Jawed, "Agronav: Autonomous navigation framework for agricultural robots and vehicles using semantic segmentation and semantic line detection," in *Proc. IEEE Conf. Comput. Vis. Pattern Recognit.*, 2023, pp. 6271–6280.
- [33] I. Alonso, L. Riazuelo, and A. C. Murillo, "Mininet: An efficient semantic segmentation convnet for real-time robotic applications," *IEEE Trans. Robot.*, vol. 36, no. 4, pp. 1340–1347, 2020.
- [34] S. Jain, X. Wang, and J. E. Gonzalez, "Accel: A corrective fusion network for efficient semantic segmentation on video," in *Proc. IEEE Conf. Comput. Vis. Pattern Recognit.*, 2019, pp. 8866–8875.
- [35] A. Ganeshan, A. Vallet, Y. Kudo, S.-i. Maeda, T. Kerola, R. Ambrus, D. Park, and A. Gaidon, "Warp-refine propagation: Semi-supervised auto-labeling via cycle-consistency," in *Proc. IEEE Int. Conf. Comput. Vis.*, 2021, pp. 15 499–15 509.
- [36] Y. Zhang, S. Borse, H. Cai, and F. Porikli, "Auxadapt: Stable and efficient test-time adaptation for temporally consistent video semantic segmentation," in *Proc. IEEE Winter Conf. Appl. Comput. Vis.*, 2022, pp. 2339–2348.
- [37] F. Yuan, L. Zhang, X. Xia, Q. Huang, and X. Li, "A gated recurrent network with dual classification assistance for smoke semantic segmentation," *IEEE Trans. Image Process.*, vol. 30, pp. 4409–4422, 2021.
- [38] G. Sun, Y. Liu, H. Ding, T. Probst, and L. Van Gool, "Coarse-to-fine feature mining for video semantic segmentation," in *Proc. IEEE Conf. Comput. Vis. Pattern Recognit.*, 2022, pp. 3126–3137.

- [39] P. Hu, F. Caba, O. Wang, Z. Lin, S. Sclaroff, and F. Perazzi, "Temporally distributed networks for fast video semantic segmentation," in *Proc. IEEE Conf. Comput. Vis. Pattern Recognit.*, 2020, pp. 8818–8827.
- [40] M. Guo, T. Xu, J. Liu, Z. Liu, P. Jiang, T. Mu, S. Zhang, R. R. Martin, M. Cheng, and S. Hu, "Attention mechanisms in computer vision: A survey," *Comput. Vis. Media*, vol. 8, no. 3, pp. 331–368, 2022.
- [41] J. Lao, W. Hong, X. Guo, Y. Zhang, J. Wang, J. Chen, and W. Chu, "Simultaneously short-and long-term temporal modeling for semi-supervised video semantic segmentation," in *Proc. IEEE Conf. Comput. Vis. Pattern Recognit.*, 2023, pp. 14763–14772.
- [42] J. Zhuang, Z. Wang, and Y. Gao, "Semi-supervised video semantic segmentation with inter-frame feature reconstruction," in *Proc. IEEE Conf. Comput. Vis. Pattern Recognit.*, 2022, pp. 3263–3271.
- [43] X. Li, K. Wang, Y. Tian, L. Yan, F. Deng, and F.-Y. Wang, "The parallelleye dataset: A large collection of virtual images for traffic vision research," *IEEE Trans. Intell. Transp. Syst.*, vol. 20, no. 6, pp. 2072–2084, 2018.
- [44] Y. Liu, J. Deng, X. Gao, W. Li, and L. Duan, "Bapa-net: Boundary adaptation and prototype alignment for cross-domain semantic segmentation," in *Proc. IEEE Int. Conf. Comput. Vis.*, 2021, pp. 8801–8811.
- [45] W. Tranheden, V. Olsson, J. Pinto, and L. Svensson, "Dacs: Domain adaptation via cross-domain mixed sampling," in *Proc. IEEE Winter Conf. Appl. Comput. Vis.*, 2021, pp. 1379–1389.
- [46] J. Li, K. Zhou, S. Qian, W. Li, L. Duan, and S. Gao, "Feature representation and reliable pseudo label retraining for cross-domain semantic segmentation," *IEEE Trans. Pattern Anal. Mach. Intell.*, pp. 1–13, 2022.
- [47] X. Wu, Z. Wu, L. Ju, and S. Wang, "A one-stage domain adaptation network with image alignment for unsupervised nighttime semantic segmentation," *IEEE Trans. Pattern Anal. Mach. Intell.*, vol. 45, no. 1, pp. 58–72, 2021.
- [48] B. Xie, S. Li, M. Li, C. H. Liu, G. Huang, and G. Wang, "Sepico: Semantic-guided pixel contrast for domain adaptive semantic segmentation," *IEEE Trans. Pattern Anal. Mach. Intell.*, vol. 45, no. 7, pp. 9004–9021, 2023.
- [49] Y. Luo, P. Liu, L. Zheng, T. Guan, J. Yu, and Y. Yang, "Category-level adversarial adaptation for semantic segmentation using purified features," *IEEE Trans. Pattern Anal. Mach. Intell.*, vol. 44, no. 8, pp. 3940–3956, 2021.
- [50] Y. Tsai, W. Hung, S. Schuler, K. Sohn, M. Yang, and M. Chandraker, "Learning to adapt structured output space for semantic segmentation," in *Proc. IEEE Conf. Comput. Vis. Pattern Recognit.*, 2018, pp. 7472–7481.
- [51] Y. Cheng, F. Wei, J. Bao, D. Chen, and W. Zhang, "Adpl: Adaptive dual path learning for domain adaptation of semantic segmentation," *IEEE Trans. Pattern Anal. Mach. Intell.*, vol. 45, no. 8, pp. 9339–9356, 2023.
- [52] M. Xu, J. Zhang, B. Ni, T. Li, C. Wang, Q. Tian, and W. Zhang, "Adversarial domain adaptation with domain mixup," in *Proc. AAAI Conf. Artif. Intell.*, 2020, pp. 6502–6509.
- [53] H. Tang, X. Zhu, K. Chen, K. Jia, and C. P. Chen, "Towards uncovering the intrinsic data structures for unsupervised domain adaptation using structurally regularized deep clustering," *IEEE Trans. Pattern Anal. Mach. Intell.*, vol. 44, no. 10, pp. 6517–6533, 2021.
- [54] W. Hong, Z. Wang, M. Yang, and J. Yuan, "Conditional generative adversarial network for structured domain adaptation," in *Proc. IEEE Conf. Comput. Vis. Pattern Recognit.*, 2018, pp. 1335–1344.
- [55] J. Shen, Y. Qu, W. Zhang, and Y. Yu, "Wasserstein distance guided representation learning for domain adaptation," in *Proc. AAAI Conf. Artif. Intell.*, 2018, pp. 10285–10295.
- [56] Q. Zhang, J. Zhang, W. Liu, and D. Tao, "Category anchor-guided unsupervised domain adaptation for semantic segmentation," in *Proc. Adv. Neural Inf. Process. Syst.*, 2019, pp. 433–443.
- [57] K. Mei, C. Zhu, J. Zou, and S. Zhang, "Instance adaptive self-training for unsupervised domain adaptation," in *Proc. Eur. Conf. Comput. Vis.*, 2020, pp. 415–430.
- [58] N. Karim, N. C. Mithun, A. Rajvanshi, H. Chiu, S. Samarasekera, and N. Rahnavard, "C-sfda: A curriculum learning aided self-training framework for efficient source free domain adaptation," in *Proc. IEEE Conf. Comput. Vis. Pattern Recognit.*, 2023, pp. 24120–24131.
- [59] X. Li, P. Ye, J. Li, Z. Liu, L. Cao, and F. Wang, "From features engineering to scenarios engineering for trustworthy ai: I&i, c&c, and v&v," *IEEE Intell. Syst.*, vol. 37, no. 4, pp. 18–26, 2022.
- [60] Y.-H. Tsai, W.-C. Hung, S. Schuler, K. Sohn, M.-H. Yang, and M. Chandraker, "Learning to adapt structured output space for semantic segmentation," in *Proc. IEEE Conf. Comput. Vis. Pattern Recognit.*, 2018, pp. 7472–7481.
- [61] L. Chen, G. Papandreou, I. Kokkinos, K. Murphy, and A. L. Yuille, "Deeplab: Semantic image segmentation with deep convolutional nets, atrous convolution, and fully connected crfs," *IEEE Trans. Pattern Anal. Mach. Intell.*, vol. 40, no. 4, pp. 834–848, 2017.
- [62] Y. Zhang, T. Xiang, T. M. Hospedales, and H. Lu, "Deep mutual learning," in *Proc. IEEE Conf. Comput. Vis. Pattern Recognit.*, 2018, pp. 4320–4328.
- [63] J. Zhu, T. Park, P. Isola, and A. A. Efros, "Unpaired image-to-image translation using cycle-consistent adversarial networks," in *Proc. IEEE Int. Conf. Comput. Vis.*, 2017, pp. 2223–2232.
- [64] A. Dosovitskiy, P. Fischer, E. Ilg, P. Hausser, C. Hazirbas, V. Golkov, P. Van Der Smagt, D. Cremers, and T. Brox, "Flownet: Learning optical flow with convolutional networks," in *Proc. IEEE Int. Conf. Comput. Vis.*, 2015, pp. 2758–2766.
- [65] T. Vu, H. Jain, M. Bucher, M. Cord, and P. Pérez, "Advent: Adversarial entropy minimization for domain adaptation in semantic segmentation," in *Proc. IEEE Conf. Comput. Vis. Pattern Recognit.*, 2019, pp. 2517–2526.
- [66] Y. Zou, Z. Yu, B. Kumar, and J. Wang, "Unsupervised domain adaptation for semantic segmentation via class-balanced self-training," in *Proc. Eur. Conf. Comput. Vis.*, 2018, pp. 289–305.
- [67] F. Pan, I. Shin, F. Rameau, S. Lee, and I. S. Kweon, "Unsupervised intra-domain adaptation for semantic segmentation through self-supervision," in *Proc. IEEE Conf. Comput. Vis. Pattern Recognit.*, 2020, pp. 3764–3773.
- [68] Y. Zou, Z. Yu, X. Liu, B. Kumar, and J. Wang, "Confidence regularized self-training," in *Proc. IEEE Int. Conf. Comput. Vis.*, 2019, pp. 5982–5991.
- [69] D. Guan, J. Huang, S. Lu, and A. Xiao, "Scale variance minimization for unsupervised domain adaptation in image segmentation," *Pattern Recognit.*, vol. 112, p. 107764, 2021.
- [70] J. Huang, S. Lu, D. Guan, and X. Zhang, "Contextual-relation consistent domain adaptation for semantic segmentation," in *Proc. Eur. Conf. Comput. Vis.*, 2020, pp. 705–722.
- [71] J. Huang, D. Guan, A. Xiao, and S. Lu, "Rda: Robust domain adaptation via fourier adversarial attacking," in *Proc. IEEE Int. Conf. Comput. Vis.*, 2021, pp. 8988–8999.
- [72] Y. Yang and S. Soatto, "Fda: Fourier domain adaptation for semantic segmentation," in *Proc. IEEE Conf. Comput. Vis. Pattern Recognit.*, 2020, pp. 4085–4095.
- [73] L. Melas-Kyriazi and A. K. Manrai, "Pixmatch: Unsupervised domain adaptation via pixelwise consistency training," in *Proc. IEEE Conf. Comput. Vis. Pattern Recognit.*, 2021, pp. 12435–12445.
- [74] K. He, X. Zhang, S. Ren, and J. Sun, "Deep residual learning for image recognition," in *Proc. IEEE Conf. Comput. Vis. Pattern Recognit.*, 2016, pp. 770–778.
- [75] J. Deng, W. Dong, R. Socher, L. Li, K. Li, and L. Feifei, "Imagenet: A large-scale hierarchical image database," in *Proc. IEEE Conf. Comput. Vis. Pattern Recognit.*, 2009, pp. 248–255.
- [76] Y. Zhang, B. Kang, B. Hooi, S. Yan, and J. Feng, "Deep long-tailed learning: A survey," *IEEE Trans. Pattern Anal. Mach. Intell.*, vol. 45, no. 9, pp. 10795–10816, 2023.
- [77] A. Kirillov, K. He, R. Girshick, C. Rother, and P. Dollar, "Panoptic segmentation," in *Proc. IEEE Conf. Comput. Vis. Pattern Recognit.*, 2019, pp. 9404–9413.
- [78] H. Ma, X. Lin, and Y. Yu, "I2f: A unified image-to-feature approach for domain adaptive semantic segmentation," *IEEE Trans. Pattern Anal. Mach. Intell.*, pp. 1–15, 2022.
- [79] A. Tarvainen and H. Valpola, "Mean teachers are better role models: Weight-averaged consistency targets improve semi-supervised deep learning results," in *Proc. Adv. Neural Inf. Process. Syst.*, 2017, pp. 1195–1204.
- [80] T.-Y. Lin, M. Maire, S. Belongie, J. Hays, P. Perona, D. Ramanan, P. Dollár, and C. L. Zitnick, "Microsoft coco: Common objects in context," in *Proc. Eur. Conf. Comput. Vis.*, 2014, pp. 740–755.



Zhe Zhang received the BS degree in the College of Information Science and Engineering, Northeastern University, China, in 2021. He is currently working toward a Ph.D. degree in the State Key Laboratory of Synthetical Automation for Process Industries, Northeastern University, Shenyang, China. His research interests include computer vision, deep learning, and working condition recognition in industrial fields.



Gaochang Wu received the BE and MS degrees in mechanical engineering in Northeastern University, Shenyang, China, in 2013 and 2015, respectively, and Ph.D. degree in control theory and control engineering in Northeastern University, Shenyang, China in 2020. He is currently an associate professor in the State Key Laboratory of Synthetical Automation for Process Industries, Northeastern University. His current research interests include image processing, light field processing, and deep learning.



many prestigious journals and conferences.

Jing Zhang (Senior Member, IEEE) is currently a Research Fellow at the School of Computer Science, The University of Sydney. He has published more than 60 papers in prestigious conferences and journals, such as CVPR, ICCV, ECCV, NeurIPS, ICLR, IEEE TPAMI, and IJCV. His research interests include computer vision and deep learning. He is also a Senior Program Committee Member of the AAAI Conference on Artificial Intelligence and the International Joint Conference on Artificial Intelligence. He serves as a regular reviewer for



Chunhua Shen is a Chair Professor with Zhejiang University.



Dacheng Tao (Fellow, IEEE) is currently a professor in computer science and an Australian laureate fellow with the Sydney AI Centre and the School of Computer Science, Faculty of Engineering, University of Sydney. He mainly applies statistics and mathematics to artificial intelligence and data science, and his research is detailed in one monograph and more than 200 publications in prestigious journals and proceedings at leading conferences. He received the 2015 and 2020 Australian Eureka Prize, the 2018 IEEE ICDM Research Contributions

Award, and the 2021 IEEE Computer Society McCluskey Technical Achievement Award. He is a fellow of the Australian Academy of Science, AAAS, ACM, and IEEE.



Tianyou Chai (Life Fellow, IEEE) received the Ph.D. degree in control theory and engineering from Northeastern University, Shenyang, China, in 1985. He became a Professor at Northeastern University in 1988. He is the Founder and the Director of the Center of Automation, Northeastern University, which became the National Engineering and Technology Research Center and the State Key Laboratory. He was the Director of the Department of Information Science, National Natural Science Foundation of China, from 2010 to 2018. He has developed

control technologies with applications to various industrial processes. He has published more than 320 peer-reviewed international journal articles. His current research interests include modeling, control, optimization, and integrated automation of complex industrial processes.

Dr. Chai is a member of the Chinese Academy of Engineering and a Fellow of International Federation for Automatic Control (IFAC). His paper titled “Hybrid intelligent control for optimal operation of shaft furnace roasting process” was selected as one of the three best papers for the Control Engineering Practice Paper Prize for the term 2011–2013. For his contributions, he has won five prestigious awards of the National Natural Science, the National Science and Technology Progress, and the National Technological Innovation, the 2007 Industry Award for Excellence in Transitional Control Research from IEEE Multi-Conference on Systems and Control, and the 2017 Wook Hyun Kwon Education Award from the Asian Control Association.